

## **Climate Monitoring SAF Cloud products feasibility study in the inner Arctic region Part II: Evaluation of variability in radiation and cloud data**

**Olavi Kärner  
Karl-Göran Karlsson**  
Visiting Scientist report - May 2003

*Front cover image:*

*Left: NOAA-14 AVHRR colour composite image (RGB) with AVHRR channel 1 as red component, AVHRR channel 2 as green component and AVHRR channel 4 as blue component from August 8 2001 at 11:11 UTC.*

*Right: Corresponding Cloud Mask image (for colour explanation, see Table 2).*

**Climate Monitoring SAF**  
**Cloud products feasibility study in**  
**the inner Arctic region**  
**Part II: Evaluation of variability in**  
**radiation and cloud data**

Visiting Scientist report - May 2003

Olavi Kärner  
Tartu Observatory, Estonia  
Karl-Göran Karlsson  
Swedish Meteorological and Hydrological Institute



## Preface

The first review (Requirements and Architectural Design Review-RADR) of the plans for the activities in the EUMETSAT Climate Monitoring Satellite Application Facility (CM-SAF) led to a recommendation from the international Review Board to consider an enlargement of the studied area including also the polar region (inner Arctic). This should at least include the processing of cloud mask and sea ice albedo parameters in order to enable monitoring of potential polar sea ice albedo changes. In response to this recommendation, the CM-SAF project team proposed to conduct a limited study (i.e., a feasibility study - not a complete development of an Arctic cloud and sea ice albedo analysis method) of inner Arctic conditions within the context of the Visiting Scientist program. The study should concern the two parameters sea ice albedo and cloud mask (the latter is a necessary parameter for extraction of the former).

Two co-ordinated activities within the CM-SAF Visiting Scientist program were proposed: one aiming at the extraction of an inner Arctic cloud mask and another for analysis of sea ice albedo. The cloud mask part was later extended to include also a preliminary study of other cloud products. This report concerns activities in the cloud products part while the work in the sea ice albedo part has previously been described by Oancea et al (2002).

Two visiting scientists, Jenny Mattson (University of Lund, Sweden) and Olavi Kärner (Tartu Observatory, Estonia), were appointed to the Inner Arctic cloud products feasibility study. The first part of the study was completed in December 2002 and results were published by Mattsson and Karlsson (2002). This report describes the second part of the study devoted specifically to a detailed cloud product evaluation.

# Contents

<b>1</b>	<b>Introduction</b>	<b>3</b>
1.1	Main Tasks . . . . .	3
<b>2</b>	<b>The main cloud algorithms</b>	<b>3</b>
2.1	CM-SAF initial AVHRR image features for cloud classifications . . . . .	4
<b>3</b>	<b>The Inner Arctic AVHRR dataset and the processing regions</b>	<b>5</b>
<b>4</b>	<b>Cloud mask determination</b>	<b>7</b>
4.1	Geometric problems in comparing satellite and ground based cloud amount estimates . . . . .	7
4.2	NOAA-16 cloud mask . . . . .	8
4.2.1	Comparison with Oden observations . . . . .	9
4.2.2	Comparison with station observations . . . . .	10
4.3	NOAA-14 cloud mask . . . . .	11
4.4	Overall summary of cloud mask performance compared to surface observations . . . . .	11
<b>5</b>	<b>Main radiative characteristics over cloudy and cloud-free areas</b>	<b>12</b>
5.1	The importance of $R_{31}$ for cloud mask determination . . . . .	14
5.2	Bias between T4 for clear pixels and NWP surface temperature . . . . .	15
5.3	On the possibility of setting an automatic threshold for T4 . . . . .	16
5.4	Sensitive threshold for dT45 . . . . .	17
5.5	On the possibility to add an algorithm for water and ice separation . . . . .	20
<b>6</b>	<b>Detailed comparison of NOAA-14 and NOAA-16 radiance measurements</b>	<b>20</b>
6.1	Difference in simultaneous brightness temperatures . . . . .	20
6.2	Comparison of CH3A and CH3B performance over the common clear areas . . . . .	22
6.3	Which is more efficient for the cloud mask: CH3A or CH3B? . . . . .	24
<b>7</b>	<b>Detailed comparison of NOAA-14 and NOAA-16 cloud masks</b>	<b>24</b>
7.1	Cloud masks during simultaneous overpasses . . . . .	24
7.2	Taking account of partly covered pixels . . . . .	26
7.3	Cloud amounts over the ARC1KM and ARC1KM_EAST areas . . . . .	27
7.4	Results from satellite-derived accumulated cloud amount statistics . . . . .	27
<b>8</b>	<b>Comparison of NOAA-14 and NOAA-16 cloud types</b>	<b>28</b>
8.1	Cloud types during simultaneous observations . . . . .	28
8.1.1	The amount of very thin cirrus as a function of dT45 . . . . .	29
8.1.2	Can very thin clouds have the same temperature difference with the surface as thick ones? . . . . .	31
8.1.3	What is the difference between low and very low? . . . . .	31
8.2	Cloud type changes during the same day . . . . .	32
8.3	Cloud type statistics from the complete satellite dataset . . . . .	32
<b>9</b>	<b>Comparison of NOAA-16 and NOAA-14 cloud top heights</b>	<b>35</b>
9.1	Cloud top heights during simultaneous observations . . . . .	35
<b>10</b>	<b>Characteristic time series for the main Arctic cloud types in summer 2001</b>	<b>36</b>
<b>11</b>	<b>Some solutions to encountered problems of cloudtop and cloud type products</b>	<b>39</b>
<b>12</b>	<b>Maximum ice extent analyses</b>	<b>41</b>
<b>13</b>	<b>Conclusions</b>	<b>43</b>
13.1	Proposal for correction of NWP modelled surface temperatures in threshold preparation . . . . .	44
<b>14</b>	<b>References</b>	<b>45</b>
<b>15</b>	<b>Appendix</b>	<b>48</b>
15.1	Used abbreviations . . . . .	48

# 1 Introduction

Clouds play an important role in the earth atmosphere. Cloud products (fractional cover, type, top height and temperature, phase, optical thickness, liquid water path) are key issues for all CM-SAF activities presenting necessary information for determining radiation budget components at larger scales. Advanced Very High Resolution Radiometer (AVHRR) measurements onboard the polar orbiting satellites are the main data source for realizing longer term operational cloud classification tasks in the polar region. The widely used philosophy (see Rossow and Schiffer 1991) that clouds are generally brighter and colder than the underlying surface does not help much over snow and ice. The albedo for snow-covered areas may be very high and the surface may have nearly the same temperature as clouds (or even colder). This means that the AVHRR CH1 (0.58 - 0.68 $\mu\text{m}$ ) and CH4 (10.3 - 11.3 $\mu\text{m}$ ) data alone cannot give enough information for cloud discrimination over snow and ice. Using all the available information provided by 5(6 for AVHRR/3) spectral channels (information shown in Table 1) is necessary to find the best method for cloud classification in Arctic. Methods based on using all spectral information were rapidly developing during the recent decade (Karlsso 1996, Stowe 1999, Kärner 2000). Among others, special methods for detecting clouds over ice and snow have been developed (Minnis et al. 2001, Chakrapani et al. 2001, Key 2002).

## 1.1 Main Tasks

This study has been initiated to investigate the possibility to extract CM-SAF cloud mask product with an acceptable accuracy on the basis of a reduced amount of polar satellite data. In addition, also the results of the cloud type and cloud top products should be evaluated. Ship measurements for selected regions and a limited set of surface observations were available to carry out detailed comparisons.

Some comments should be useful. It is generally accepted that a method satisfactory to every user is still not available. This means that any comparison of cloud products based on data from different satellites should start from an explanation of the methodical difference. After that the cloud products can be compared. Especially, NOAA-14 and NOAA-16 observations of the inner Arctic test area during the same time can be used for that purpose. The results can present additional information to estimate the accuracy of products. Validation of the satellite cloud amounts using surface observations can not be extensive over this region almost without operational meteorological observations.

## 2 The main cloud algorithms

The CM-SAF cloud algorithms are based on the algorithms developed by the EUMETSAT SAFNWC project (see [www.smhi.se/saf/](http://www.smhi.se/saf/)). In principle, the cloud mask and cloud type algorithms are both elaborate threshold methods which use all AVHRR information. The CM-SAF cloud mask algorithm is a unique one among other algorithms. Most of the algorithms (Rossow and Schiffer 1991, Stowe et al 1999, Key 2002) are trying to find generally applicable optical parameters which are able to produce a satisfactory contrast between cloudy and cloud-free situations. Surface temperature is ordinarily the only ancillary parameter applied. The CM-SAF scheme is produced on the basis of other principles: temperature and humidity conditions for every remotely sensed pixel should be known *a priori*. This means that clouds are to be detected in real synoptic conditions instead of any (hypothetical) mean atmosphere. Implementing the idea brings about an extensive preprocessing for getting dynamical threshold values on the basis of short range numerical weather prediction (NWP) gridded datasets.

Table 1: AVHRR/3 spectral channels

Channel No.	Wavelength ( $\mu\text{m}$ )
1	0.58 - 0.68
2	0.725 - 1.00
3A	1.58 - 1.64
3B	3.55 - 3.93
4	10.3 - 11.3
5	11.5 - 12.5

Table 2: Cloud mask categories, their code numbers and corresponding product colours (see front cover) during the experiment.

Category nr	Category name	Colour
0	<i>Non processed</i>	Black
1	<i>Cloud free</i>	Green(land)/Blue(sea)
2	<i>Cloud contaminated</i>	Grey
3	<i>Cloud filled (opaque)</i>	Orange
4	<i>Snow/ice contaminated</i>	White blue
5	<i>Unclassified</i>	Red

Table 3: Cloud types and their code numbers during the experiment.

Type nr	Type name
0	<i>Not processed</i>
1	<i>Cloud free land</i>
2	<i>Cloud free sea</i>
3	<i>Snow/ice contaminated land</i>
4	<i>Snow/ice contaminated sea</i>
5	<i>Very low clouds</i>
7	<i>Low clouds</i>
9	<i>Medium level clouds</i>
11	<i>High and opaque clouds</i>
13	<i>Very high and opaque clouds</i>
15	<i>Very thin cirrus clouds</i>
16	<i>Thin cirrus clouds</i>
17	<i>Thick cirrus clouds</i>
18	<i>Cirrus clouds above low or medium level clouds</i>
19	<i>Fractional or sub-pixel clouds</i>

The best possible prediction of the cloudfree scene using radiative transfer models (RTM) together with the best available guess of the actual atmospheric state is included (Dybbroe et al. 2000). A condensed form of the algorithm structure is presented in Dybbroe et al. (2002) while more details are provided in Dybbroe et al (2003). For a clearer understanding of the discussion in this report, the output from the two basic cloud products cloud mask and cloud type are repeated above in Tables 2 and 3.

## 2.1 CM-SAF initial AVHRR image features for cloud classifications

A list of the features used by CM-SAF for cloud detection is presented. The main features are often used by different authors. The corresponding threshold values (if constant for the Arctic region) are selected and presented also.

- Visible (CH1) bi-directional reflectance (hereafter R1).
- Pseudo-visible (CH1) reflectance (assuming sun in zenith).
- Local (5×5) standard deviation for R1.
- Near-infrared (CH3A) bidirectional reflectance R3A. The new AVHRR, flying on NOAA K,L,M satellites has an additional channel-three, usually labelled as CH3A, specially designed for better snow and cloud discrimination. It's usefulness for snow cloud and sunglint discrimination has previously been tested by Hyvärinen et al. (1999).
- Near-infrared (CH3B) bidirectional reflectance R3B. The reflection of solar radiation in this band is very weak by the earth surface (including snow and ice). Clouds reflect essentially more, providing an opportunity for the discrimination. R3B is assumed to be correctly estimated

after subtraction of the emitted radiation in CH3B computed by using the infrared brightness temperature in AVHRR channel 4 (T4).

- Near-infrared ( $1.6\mu\text{m}$ ) and visible reflectance quota  $R_{31}=(R3A/R1)$ .
- Reflectance ratio  $R_{31}^*=R3B/R1$ .
- Near-infrared (CH3B) brightness temperature (T3B - hereafter, if a channel number follows, the term always stands for brightness temperature).
- Infrared (CH4) T4.
- BT difference CH4 – CH3,  $dT43=T4 - T3$ . The most frequently used feature (in both directions:  $dT34$  or  $dT43$ ) For  $dT34$ , Minnis et al. (2001) present the following values —  $8.6\pm 1.8\text{K}$ ,  $5.7\pm 1.3\text{K}$ ,  $5.4\pm 2.6\text{K}$  found for May, June, July, respectively during the First ISCCP Regional Experiment (FIRE) Arctic Cloud Experiment (ACE) over  $8^\circ$  latitude and  $30^\circ$  longitude domain. Chakrapani et al. (2001) obtained different threshold values for sea and land conditions over the same region. Their results are somewhat lower (about 4K for sea and 7K for land). In the present text any confusion can be avoided recalling that CH3A is used in  $R_{31}$  and CH3B in  $dT34$ .
- Local ( $5\times 5$ ) CH4 BT standard deviation.
- BT difference CH4 – CH5,  $dT45$ . Most difficult feature to use due to its dependence on temperature, water vapor amount and satellite viewing angle (see special section later for details).
- BT difference CH3B – CH5,  $dT35$ . This feature is to a large extent similar to the previous one and share the same difficulties in its use.
- Local ( $5\times 5$ ) standard deviation for BT difference CH3B – CH5.

### 3 The Inner Arctic AVHRR dataset and the processing regions

In this study, a data set collected during the Oden Arctic Ocean 2001 summer expedition has been used (see <http://www.polar.se/english/expeditions/previous.expeditions.html>). The NOAA AVHRR part of the data set consisted of in total 194 NOAA LAC scenes from July 2 to August 28 from which a subset of scenes was selected.

To increase the amount of useful LAC scenes compared to the data set previously used by Mattsson and Karlsson (2002) in part I of this study, a shift of the processing region was found necessary. Consequently, in addition to the previously used region ARC1KM a new region ARC1KM.EAST was introduced. Both regions are described in Fig. 1.

The finally selected and studied subset of LAC scenes consisted of 90 AVHRR scenes (45 NOAA-14 scenes and 45 NOAA-16 scenes) from both the old AVHRR/2 sensor and the new AVHRR/3 sensor. The scenes were chosen with the purpose of having one NOAA-14 and one NOAA-16 observation from each day covering the same area with as little time difference as possible. The purpose of this choice of scenes was that it would then be possible to investigate the impact on the cloud detection and cloud analysis results due to the change from the AVHRR/2 instrument on NOAA-14 to the AVHRR/3 instruments on NOAA-16. The new AVHRR/3 sensor provides data from a new 1.6 micron channel (denoted AVHRR channel 3A) which was originally motivated and introduced for having the highest potential for cloud/snow discrimination.

Most NOAA-14 scenes had overpass times close to 12 UTC while corresponding NOAA-16 scenes had overpass times close to 09 UTC. A few NOAA-16 scenes with overpass times close to 03 UTC were included but also some scenes with only a few minutes time difference compared to NOAA-14 overpasses.

Figure 2 shows the overall coverage of LAC scenes in area ARC1KM.EAST for the two satellites based on the selected 90 LAC scenes. Some differences in coverage could be seen. NOAA-14 has best coverage in the central and lower part of the region while NOAA-16 coverage is best in the central upper portion of the area, mainly due to the presence of a number of nighttime scenes (close to 03 UTC) with a different overpass orientation compared to the other overpass times.

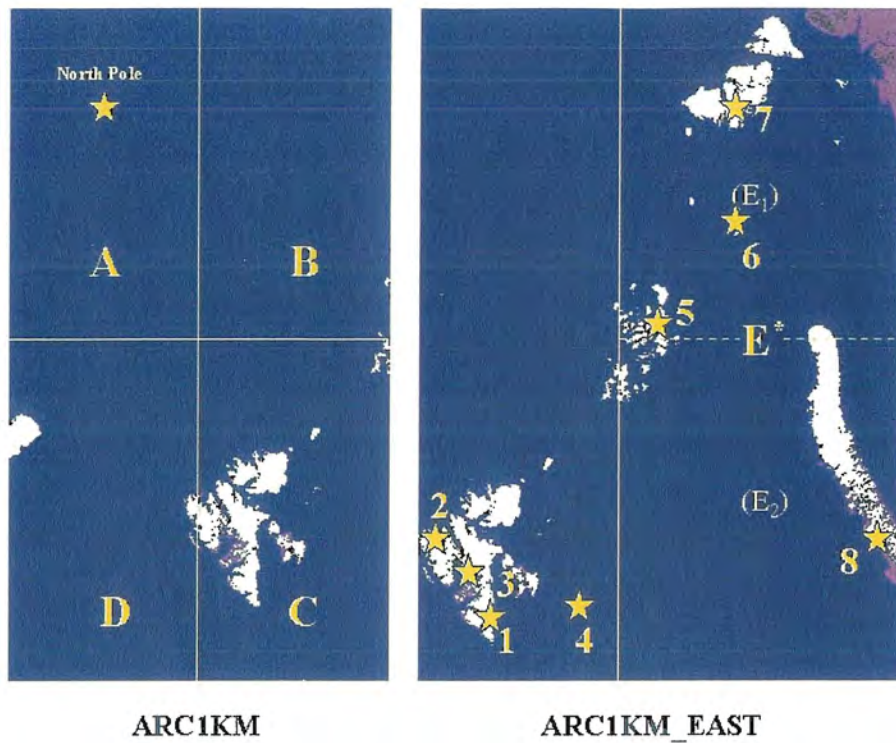


Figure 1: Processing areas ARC1KM (left) and ARC1KM.EAST (right) and the disposition of sub-areas (letter notations are explained in the text). The position of the North Pole and the positions of the used synoptical surface stations are indicated as stars (see also Table 5).

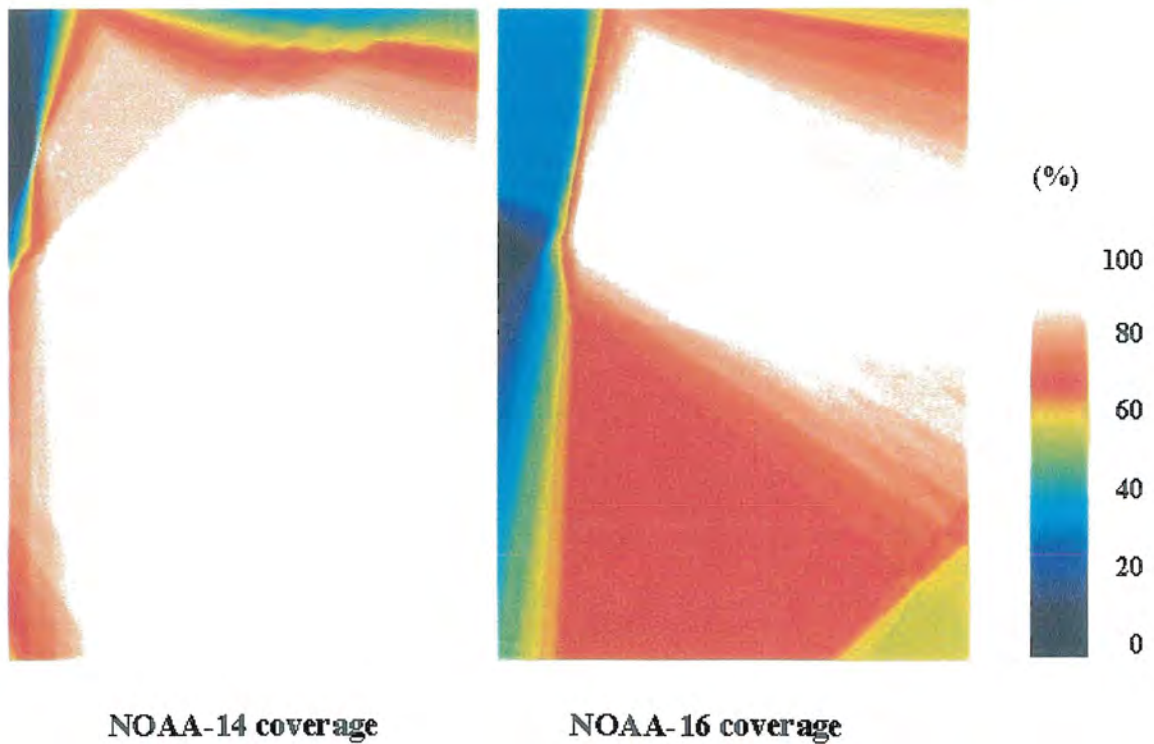


Figure 2: Coverage of NOAA-14 scenes (left) and NOAA-16 scenes (right) in processing region ARC1KM.EAST (see Fig 1) by the selected LAC data set.

For validation purposes, observations from 8 synoptical surface stations in the Arctic region have been used (marked out by numbers in Fig. 1). Previously, a limited ground observation data set from the Oden ship were used in the first part of the Inner Arctic Cloud Products Feasibility study (reported by Mattsson and Karlsson, 2003).

All necessary auxiliary information (e.g. NWP data) was identical to the information previously used by Mattsson and Karlsson (2002).

## 4 Cloud mask determination

In the present report cloud mask is the set of pixels which contains all cloudy and cloud contaminated pixels. No portioning to overcast and partially covered pixels occurs. This means that the cloud mask area for any scheme is generally larger (and never smaller) than the simultaneous total cloud amount on the same region. The CM-SAF cloud mask calculations for the ARC1KM area are described in detail by Mattsson and Karlsson (2002). Here, some statistical analysis is carried out in order to study the reliability of the mask in respect to some theoretically known (and practically verified) spectral properties allowing any distinction between cloudy and clear pixels. CM-SAF cloud detection results are analyzed over two partly overlapping areas (see Fig 1).

The first one - ARC1KM - was initially chosen. During the present study this area was divided into four sub-areas ( $A, B, C, D$ ) in order to catch possible differences in radiative properties over (mainly) water and ice-covered surfaces. Actual overlapping of the NOAA-16 and NOAA-14 registered data files appeared to be insufficient. This led to the introduction of another testing area called ARC1KM\_EAST (hereafter labelled as  $E$ ), which has some overlapping of the previous one but guarantees at least twice more common pixels for the analysis.

### 4.1 Geometric problems in comparing satellite and ground based cloud amount estimates

Ground-based observations are indispensable in order to get information about actual cloud types during the satellite measurements. Unfortunately, this information is not complete. If low cloudiness is extensive, higher levels are not observable.

But if one wants to test satellite cloud amount results using ground based amounts as reference even larger difficulties arise. The problem how to find a satisfactory relationship between ground based and satellite derived cloud amounts has been popular long before the actual satellite cloud detection became operational (Appleman 1962, Lund 1965, Avaste et al. 1972, Malberg 1973). The problem appears to be unsolvable on the basis of existing information and the key issue is a nonzero cloud thickness. The ground observer is much closer to cloud field than a satellite sensor, and his cloud amount estimate is primarily defined by the situation near the zenith. Besides this, cloud sides tangle to see all the spaces between clouds. Side effects for the ground observer increase from center towards the margins. Side effects for satellite sensor may also be remarkable (scanning zenith angles up to 70 degrees) but they are practically constant over the areas comparable to those visible from surface. As a result, estimated cloud amounts by a ground observer are generally larger than those by satellites. Avaste et al (1972) modeled cumulus clouds using different shapes (cylinder, box etc) and different distribution of cloud base centers in order to estimate the overestimation. They put satellite at the zenith and fed various distribution of model clouds with predetermined (absolute in orthogonal projection) cloud amount values for some model area and calculated apparent amounts for the ground observer situated in the center of that. In order to explain the dependence on cloud thickness, the calculations were carried out for cloud fields with constant thickness in every case. Figure 3 shows the result for two cloud thickness values 0.1 km and 1.0 km.

Figure 3 shows that strong overestimation occurs in case of small and moderate (absolute) cloud amount. For clear and overcast cases both projections lead to the same result, naturally.

Malberg (1973) carried out an extensive comparison of mean cloud cover obtained by satellite photographs and ground-based observations over Europe and Atlantic. His conclusion was that for high latitudes (over 70° N) the overestimation for large scale averaged might be about 0.09.

During recent years it is expected (Minnis et al. 2001) that ground-based and satellite determination should yield very similar mean cloud amounts for a significant number of samples. The expectation is partially supported by general properties of cloudiness distribution in the earth atmosphere. Cloud areas are generally much wider than the area visible by a ground observer. This leads to U (or J) type density function for cloud amount probability for small areas (e.g. Falls 1974). Averaging over

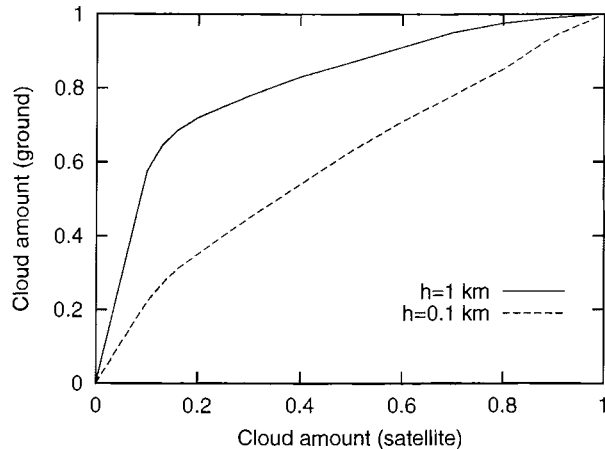


Figure 3: Overestimation of ground based cloud amounts depending on cloud thickness (Avaste et al. 1972)

large samples gives more value for both ends (clear and overcast) which are not contaminated for any ground observer. But total elimination of the cloud side effects in ground observations is impossible because they all indicate one and the same direction. On the other hand, there holds a simple compensation mechanism in satellite techniques: counting cloud contaminated pixels as overcast leads also to an overestimation of cloud amount. Good accordance, sometimes found between the compared cloud amounts (e.g Minnis et al.2001, Schweiger 1999) is a result of these effects. Both approaches are overestimating due to inability to treat partially cloudy field of view properly.

Recent experience over the Scandinavian region (Karlsson 1996, Karlsson 2001 and Karlsson 2003) indicates that the surface overestimation normally dominates over the satellite overestimation during the summer half of the year. This is explained by the fact that summertime convective cloud elements have larger vertical dimensions than what could be seen for other parts of the year. Consequently, the risk for surface overestimation of the cloud amount increases (see Figure 3). Since we do not expect to find convective cloud elements with large vertical dimensions in the inner Arctic region during the studied period, the surface overestimation effect will probably be small. Thus, the importance of the potential satellite overestimation could be higher.

Due to the geometry aspects, any fitting of satellite cloud amounts to ground observed amounts may lead to biased values (i.e overestimation). Another (and also permanent) source of error, connected to the ground based cloud amounts is accuracy. Obtained amounts by a ground observer are visually estimated, not measured. These values have been used to approximate cloud influence to solar radiation reaching the earth's surface by many authors starting from Ångström (1924). But the results vary essentially (see Table 8.1 in Kärner and Keevallik 1993). It can be expected that a large part of the variation is due to cloud observation errors and only smaller part due to variations in cloud optical thickness. The CM-SAF tasks demand accurate measurements of cloud properties. Subjective and visual estimations of such properties are largely unfit to provide the information that is needed here. More discussion about this problem follows in the final conclusion section.

But there are still some special cases presenting essential interest for comparison:

1. Cloud-free areas. If sufficiently large, their radiative properties are important for testing the reproduced threshold values over the vicinity.
2. Overcast areas can be used for similar purpose – to study radiative properties of cloud fields. They have also (partial) importance for determining (low) cloud types. But those may be not detected by satellite.
3. Partially cloud covered fields of view are useful for type testing.

## 4.2 NOAA-16 cloud mask

NOAA-16 cloud mask calculations and the estimation of cloud amounts at specific positions of surface observations in the ARC1KM area are described in detail by Mattsson and Karlsson (2002). Here, some statistical analysis is carried out in order to study the reliability of the mask in respect to some theoretically known (and practically verified) spectral properties allowing any distinction between

Table 4: Oden observations and the corresponding CM-SAF cloud products for  $31 \times 31$  pixel regions

Date	Time (UTC)	Lat	Lon	octa/type	CM-SAF octa/level
07.10	10.07	82.0	26.8	8 St+Ns	8 low
07.11	11.38	81.3	24.5	6-8 St+mist	8 medium + Ci
07.24	04.08	87.6	131.0	8 St	8 low
07.26	03.47	87.6	144.0	0 mist	0
07.27	03.36	87.9	154.0	1 Ac	6 low + fractional
07.28	03.25	87.8	150.0	0 mist	8 low + medium
07.30	03.04	89.5	158.0	8 St	8 medium + Ci
08.02	04.14	89.0	0.2	8 St+Sc	8 very high

cloudy and clear pixels.

#### 4.2.1 Comparison with Oden observations

This dataset has been collected during the two-month (July-August) Arctic expedition with the Swedish ice-breaker Oden in 2001. It includes both ship measurements of basic cloud parameters (amount, type, base height) and of broadband surface albedo. Cloudy scenes are prevailing in the inner Arctic during summer (see also summary results in section 7.4). Thus, the overcast cases present major interest for comparison.

The work was planned to collect histograms for four variables over the vicinity of Oden during satellite overpasses when the Oden observer had registered overcast situation. The chosen variables are: Channel 3A bidirectional reflectance ( $R_{3A}$ ), normalized cloud index (NCI), where  $NCI = (R_1 - R_{3A}) / (R_1 + R_{3A})$ , Saunders and Kriebel (1988) introduced ratio  $R_{21} = R_2 / R_1$ , and split-window brightness temperature difference  $dT_{45} = T_4 - T_5$ . Reflectance in all wavelengths depends more or less on the solar and viewing angles. The NCI is chosen to decrease that dependence. Key (2002) calls the same index as Normalized Difference Snow Index, but our primary concern is cloud detection. There still remains a problem of misinterpretation, if snow or clouds in shadow are tested. In both cases  $R_1$ ,  $R_{3A}$ , and NCI are small,  $R_{31}$ , as a ratio of two small values, is arbitrary. There is a scarce information about performance of the  $R_{21}$  over snow and ice. New collections might be useful for estimating the distinction between pack ice and open ocean. Oden coordinates are serving as the center of a  $31 \times 31$  pixel subimages over that the cloud and radiation data are averaged. Possible navigation errors are ignored. The results are interpreted as estimates of the CM-SAF cloud algorithm accuracy in Arctic conditions. Ship observations values are treated as true.

Actually, there were only 8 cases during NOAA-16 observations when the satellite swath covered Oden in overcast or clear conditions. Partially covered area around Oden can not provide useful information for estimating cloudy radiance distribution. Results of the cloud type and amount comparison for these 8 cases are presented in Table 4.

In 3 cases the ship observer registered almost clear: once 1 octa Ac and twice mist. The result according to CM-SAF algorithm was different. One mist case was defined clear, another overcast by stratiform clouds. One octa Ac case was classified as partly cloudy with cloud amount 0.714. The result probably indicates a navigation error, because the CM-SAF detected cloud front has a straight line near the expected Oden position. About 10 km shift of the picture, and the ground-based 1 octa case can be easily reproduced. Thus, the comparison results are not contradicting but explaining the difficulties one needs to overcome if planning any use of surface based observations to validate a satellite cloud detection scheme.

Both sources agree showing overcast in 5 cases. This enables us to test the behaviour of visible and near-infrared radiances over these boxes. Collected frequency distributions for NCI,  $R_{31}$  and  $R_{21}$  are presented in Fig 4.

Figure 4 shows that theoretical expectations (e.g Hyvärinen et al. 1999, Key 2002) for cloudy conditions ( $NCI < 0.5$ ,  $R_{31} > 0.3$  and  $R_{21} > 0.75$ ) are all satisfied. But for 17% of pixels  $R_{21} > 1.35$ . Theoretically (Saunders and Kriebel 1988), such values characterize vegetated land. All the compared boxes were far from any land. The obtained departure must be due to special atmospheric or cloud distribution conditions. Visual inspection of images suggests that shadowing effects in situations with layered clouds at various altitudes might be responsible for a substantial part of these deviations. Shadowing effects appear to be capable to substantially alter the 'typical' cloud signatures. The most

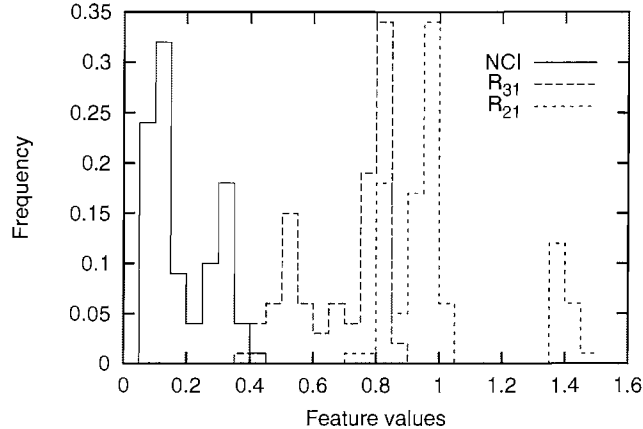


Figure 4: Frequency distributions for three features over 5 scenes where Oden and satellite estimates show overcast.

difficult condition appears to be created when high-level clouds cast shadows on low-level clouds and when at the same time very thin Cirrus clouds are superposed over this shadow.

#### 4.2.2 Comparison with station observations

There are 7 ground observations by different stations over the  $E$  area (see station positions in Fig. 1) reporting almost clear (i.e cloud amount not more than 2 octas) situations while the time interval with NOAA-16 overpass was less than 1 hour. The situation enables us to compare CM-SAF, station data and  $R_{31}$  estimates in practically cloud-free conditions. CM-SAF cloud mask results are in good accordance with the station data (average values 0.132 and 0.178 respectively, the latter computed from the average octa value). But the frequency distribution for  $R_{31}$  shows long tail towards high index values (in 20 % of cases  $R_{31} > 1.0$ ) This may contradict the theoretical expectation (e.g Key 2002) that R3A is low for clear land and water. For more detailed study, the CM-SAF classification for clear areas is used to separate  $R_{31}$  frequency distributions into three classes (land, water and ice). The two first of them can present necessary information about the difference of  $R_{31}$  distribution over various surface types. The third is closely connected to the value of the same feature and cannot help in separation. Frequency distributions for  $R_{31}$  gathered up over clear land and water pixels from the stations vicinity in cloudfree cases show similar behaviour:  $R_{31} < 0.3$  is satisfied for 18% of land and 73% of water pixels. Condition showing the other margin  $R_{31} > 1.0$  is satisfied by 45% of land and 10% of water pixels. Here, only the pixels which are clear by CM-SAF and station observations in the vicinity of  $31 \times 31$  pixels are accounted for. The reason of a strong increase in  $R_{31}$  cannot be due to favourable situation in viewing and relative azimuth angles. Testing areas around the stations are too small to allow big differences. For Aug. 07 the viewing zenith angle (VZA) is in the interval from 0 to 30 degrees and relative azimuth angle (RAZ) from  $-120$  to  $-100$  degrees, the condition which does not support sun glint. In addition to that, large values in  $R_{31}$  are much more frequent over land.

Trepte et al (2001) report quite rapid increase in R3A if VZA exceeds  $50^\circ$ . In order to test that frequency distributions for VZA and RAZ are gathered for four orbits over  $E$  if  $R_{31} > 0.9$  and CM-SAF defined clear pixels. The total number of such pixels was 17828. The results do not support any special dependence of  $R_{31}$  on VZA. The frequency of high  $R_{31}$  value for near nadir VZA ( $0 - 15^\circ$ ) is approximately the same as that for near swath edge ( $60 - 75^\circ$ ). The reason why these pixels seem clear for CM-SAF is in R1 and T4. They are generally dark (96% of them have  $R1 < 12\%$ ) and warm (71% are warmer than the adjusted clear/cloud contaminated threshold value). Some scepticism about the clear status may remain. Possibly, as mentioned before related to the behaviour of the  $R_{21}$  feature, complicated shadowing effects may have distorted feature values making them more similar to their cloud-free appearance. We shall return to these pixels later when comparing NOAA-16 and NOAA-14 based products during simultaneous overpasses.

In addition to that, any existence of rare haze near the surface might be among the reasons. The problem with an increased dT34 for cloudfree sky and its probable relation to the enhanced reflection of CH3B due to arctic haze over SHEBA region is reported by Spangenberg et al. (2001). Trepte et al (2001) expect a similar reflectance increase for R3A.

Feature  $R_{21}$  behaves even more controversially over these testing sites. The condition  $R_{21} < 0.75$ , expected to hold for clear water, is satisfied for 18% of clear land and only 4% of clear water pixels. Cloudy (or ice) scenes can be expected (i.e.  $0.75 < R_{21} < 1.2$ ) for 51% of land and 10% of water pixels. Clear land can be expected for 31% of land and 86% of water pixels during the comparison of these 7 cases. As a result, using visible channels only may not lead to any successful cloud detection over mixed water and land areas in a summertime Arctic. The behaviour of  $R_{21}$  over the same pixels appeared to be controversial also. The only found tendency is that  $R_{21}$  supports more groundtruth results over land (31%) and  $R_{31}$  over water (73%).

### 4.3 NOAA-14 cloud mask

NOAA-14 cloud mask calculations and the estimation of cloud amounts at specific positions of surface observations in the ARC1KM area are described in detail by Mattsson and Karlsson (2002). Here, some results of comparisons with station cloud observation data are presented in order to characterize the CM-SAF ability of distinction between clear and cloud contaminated situations. There were 7 cases over  $E$  area with the station reporting totally cloud-free conditions over their visibility region and 27 cases with low cloud amount (1 to 2 octas). The time difference between the station observation and NOAA-14 overpass was generally less than 1 hour. These conditions are sufficient for getting useful information about the CM-SAF cloud scheme performance in cases of slight cloud contamination. Due to cloud side effects, all other cases may give biased estimates, and any direct comparison is not sufficiently reliable. In addition to the CM-SAF cloud mask value also the frequency distribution for dT34 is calculated over the stations vicinity.

In 6 cases from total 7 where station observers reported clear the CM-SAF shows very close results (average cloud amount value over  $31 \times 31$  pixel area is 0.03). Also 94 % of pixels have their dT34 value less than 6 K, which is in excellent accordance with those by clear scenes. But one comparison (NOAA-14 overpass 23.07 12.44 with station 20062 - station number 5 in Fig. 1 - observations at 12.00 GMT) gives contradictory results. NOAA-14 data show 99.3 % cloud amount (cloud contamination by types 9 and 19 - see Table 3) instead of expected clear. dT34 values support that: values are mainly from 15 to 24 K. Also visual inspection of result images as well as the original AVHRR channel images support the result of the cloud mask. There may be several explanations: rapid cloud formation during previous 45 minutes, enhanced reflectance of CH3B due to haze (similar condition as reported by Spangenberg et al. (2001), large navigation error for satellite data, or error in the station report. The latter may be quite likely, because the neighbouring observations at 9 and 15 GMT for that day and station are not registered in the dataset.

27 almost clear cases give good accordance between the values from the three sources. The average station cloud amount is 0.157 and that by CM-SAF 0.135. These results are supported by dT34. The latter cloud mask is estimated using previous experience (Karlsson 1996, Kärner 2000) that the pixels with  $dT34 < 6$  K are probably clear and those with  $6 < dT34 < 12$  K are probably cloud contaminated. Counting the corresponding pixels gives the cloudy amount equal to 0.07 and the contaminated amount equal to 0.15. Summary cloud mask estimate of 0.22 is in reasonable accord with the values by stations and CM-SAF. A summary of the comparison with station report results for nearly cloudless situations is shown in the Appendix Table 22. The table shows observation time, station coordinates, time difference in minutes between the station observation and satellite overpass, station observers report on cloud amount in octas, cloud type, cloud base height and the CM-SAF results on total cloud mask (cm) and cloud type, respectively. The results confirm that the ability of CM-SAF for cloud mask determination is good. It could be mentioned that there is a tendency in CM-SAF scheme to find cloud type 19 (fractional clouds) while the station observer reports pieces of cirrus clouds.

### 4.4 Overall summary of cloud mask performance compared to surface observations

As a final rough check on the overall cloud mask performance, results from a general comparison with all available surface observations (from the 8 stations previously described in Fig. 1) are shown in this section. Notice here that in this calculation of cloud amounts cloud-contaminated pixels have been counted as fully cloudy. Results from individual stations are given in Tab. 5 and a summary for the total data set and splitted into one NOAA-14 and one NOAA-16 part is given in Tab. 6. Here, only surface observations within one hour time difference from satellite overpass have been used.

Table 5: Comparison of surface-observed total cover and satellite-estimated cloud cover from cloud-mask results in a 33x33 pixel neighbourhood centered at each surface station position. Results are based on the difference SATELLITE minus SURFACE cloud amount.

Number	Station number	Latitude	Longitude	Bias (%)	st. dev.	Samples
1	01003	77.0	15.5	-4.2	17.8	49
2	01007	78.92	11.93	4.5	7.9	18
3	01008	78.25	15.47	-0.3	13.5	52
4	01062	76.5	25.07	-16.7	33.7	45
5	20046	80.62	58.05	3.1	27.1	25
6	20069	79.5	76.98	3.0	15.3	22
7	20087	79.55	90.62	-0.0	17.4	22
8	20744	72.37	52.7	-7.1	14.5	27

Table 6: Summary results from the comparison of surface-observed total cover and satellite-estimated cloud cover (SATELLITE minus SURFACE).

Selection	Bias (%)	st. dev.	Samples
All samples	-3.6	20.9	260
NOAA-14 samples	-3.4	20.2	221
NOAA-16 samples	-5.3	24.1	39

The overall results suggest that there is a slight satellite underestimation of cloud amounts which is, to some extent, contradicting the expectation of a small satellite overestimation of cloud amounts in the Arctic region during the summer season (see discussion in the previous section 4.1). There is a very strong negative component from one of the eight stations (number 4 with station number 01062) and it is possible that results are too negatively biased due to special conditions or problems for this particular surface station. At this moment, the special characteristics of this station are not known.

If disregarding station 4, results show very good agreement with observed cloud amounts. However, since a more pronounced satellite overestimation of cloud amounts could be expected for non-convective cloud conditions (following the discussion in section 4.1) we suspect that there are still some clouds that have remained undetected in the results. This is also indicated in the previous sections 4.2 and 4.3 showing some deviations from the 'normal' cloud-free appearance of water and land surfaces.

The separation of the groups NOAA-14 samples and NOAA-15 samples, respectively, does not reveal any significant difference between the two groups. Some sign of a increased negative bias is seen for NOAA-16 but since the number of samples for this group is considerably lower than for NOAA-14 it is not possible to make any firm conclusions.

The overall results support other validation reports for Arctic conditions (Dybbroe et al, 2003) showing a tendency of a slightly decreased cloud detection capability in the Arctic environment, especially in cases of high solar zenith angles (twilight conditions).

## 5 Main radiative characteristics over cloudy and cloud-free areas

An approximate performance of the method can be tested by calculating frequency distributions for the variables theoretically important for clear/cloud distinction. Two types of surfaces, water and ice are of interest during the Arctic summer. Thus,  $R_{31}$  and  $R_{21}$  are likely to present useful tools for distinction between clear and cloud contaminated scenes. The first of them is a part of the variables used by CM-SAF itself, but not the decisive one. Its performance can give an impression of its importance in the whole process. NCI performs very similar in comparison with  $R_{31}$  and using both of them does not add new information.

Cloud detection differences over water and ice may be remarkable. The whole testing operation is carried out in two phases. In the first phase four separate sub-areas (see Fig. 1) in the ARCIKM

Table 7: Fraction of  $R_{31} < 0.3$  and  $R_{21} < 0.75$  values over CM-SAF cloud mask components

CM-SAF determined	Area	amount of pixels n	$R_{31} < 0.3$	$R_{21} < 0.75$
<i>clear</i>	A	869171	0.980	0.403
-	$B_1$	716962	0.933	0.423
-	$B_2$	626142	0.893	0.456
-	C	1 235815	0.636	0.823
-	D	418527	0.721	0.822
<i>ice</i>	A	79229	-	0.414
-	$B_1$	795594	-	0.436
-	$B_2$	237528	-	0.583
-	C	363663	-	0.500
-	D	509913	-	0.550
<i>cloud</i>	A	2 835100	0.037	0.019
-	$B_1$	3 406104	0.093	0.027
-	$B_2$	3 112661	0.038	0.018
-	C	3 952055	0.035	0.005
-	D	1 772660	0.026	0.010

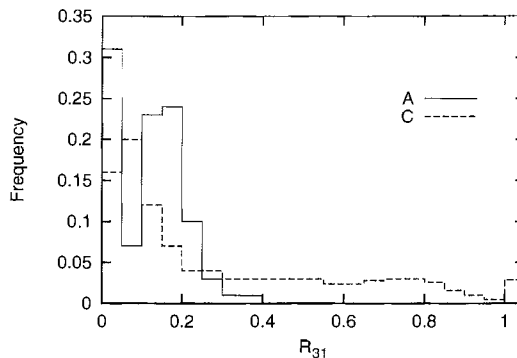


Figure 5: Frequency distribution for  $R_{31}$  values over CM-SAF defined clear pixels for two sub-areas

region are used, and in the second phase one (large) ARC1KM\_EAST area was considered. In the first phase the sub-areas A and B were mainly ice-covered during the experiment and two others (C and D) were mainly ice-free. Histograms for  $R_{31}$  and  $R_{21}$  in three conditions of the target (clear land or water, cloud, ice-contaminated land or water) determined by the CM-SAF scheme are collected over four areas. The B area is scanned two times more than the others (i.e. during both the night and morning overpasses). Hereafter,  $B_1$  stands for night observations and  $B_2$  for morning ones. Cumulated results in respect to the expected clear/cloud contaminated threshold values are shown in Table 7.

Table 7 shows that the used  $R_{31}$ -condition for clear pixels  $R_{31} < 0.3$  holds perfectly over the A sub-area. Only 2% of the pixels declared as being clear by the CM-SAF scheme have  $R_{31} > 0.3$ . The amount of cloudy pixels showing  $R_{31} < 0.30$  is even less over the same area. Over the other areas the situation is more complicated. The amount of pixels where  $R_{31} > 0.3$  increases slightly over the clear areas of B regions, but (seemingly) too much over C and D. There is a nonzero fraction of the region where  $R_{31} > 1$ , leading the ratio to exceed unity. As an illustration,  $R_{31}$  frequency distribution collected for clear pixels over two sub-areas, A and C are shown in Fig. 5. All the cases where  $R_{31} > 1$  are collected to one and only bin (1 – 1.05) and it gathers a remarkable frequency. Figure 5 shows that the cases with enhanced CH3A reflectance are quite frequent in the Arctic conditions.

For cloudy areas (by CM-SAF)  $R_{31}$  shows reasonably good (in terms of the theory) performance over all areas. Amount of controversial cases is clearly less than 10% (Table 7). CM-SAF uses the condition  $R_{31} < 0.3$  as the crucial one to determine ice and the comparison makes no sense in this special case.

Performance of  $R_{21}$  has stronger dependence of the underlying surface. Last column results may be interpreted as follows: there may be less ice and more water surface among clear pixels over C and D sub-areas. That is why the condition  $R_{21} < 0.75$  is satisfied more frequently. The problem of water

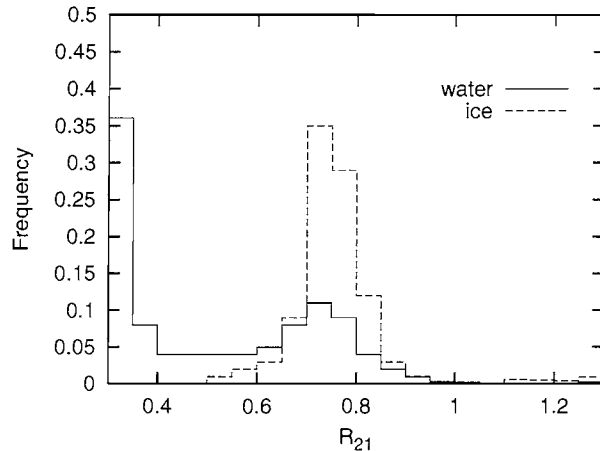


Figure 6: Frequency distribution for  $R_{21}$  values on CM-SAF defined cloudfree water and ice regions over  $C$  sub-area

and ice separation will be further treated in more detail.

Figure 6 shows frequency distribution for  $R_{21}$  over  $C$  sub-area separately for CM-SAF determined water and ice pixels. The first one has a behaviour similar to the theory: Main part of the ratio is less than 0.75. But non-zero frequencies reach to the value 1.35. A curve, quite similar to that for cloud (see Fig 4) is obtained for the ratio in case of ice contaminated clear region. The mode is situated near the theoretical water/cloud threshold (0.75). The frequency of the values  $R_{21} > 1.2$  is also remarkable. Abundance of the values theoretically belonging to vegetated land does not support the use of that feature. The distribution for clouds (not shown) shows even more pixels with the ratio value theoretically corresponding to vegetated land. These cases require more careful study. The reason should reside in the upper tropospheric optical properties or, alternatively, or in cloud shadow effects.

Considering shortwave channels, two (slightly controversial) conclusions are important:

- $R_{31}$  behaviour is generally according to the theory. CH3A has been designed for cloud separation over snow and ice, so it performs better over  $A$  than anywhere else. A remarkably weaker ability over water and land surface is noticed. Here,  $R_{31}$  frequency distribution has a long tail towards larger values reaching far beyond 1.0 for CM-SAF and ground station found cloud-free cases. The relation of that tail to the viewing geometry seems to be quite weak. No evident sunglint was found. The signal was a bit lower over the sub-area  $A$  and  $B_1$  during night overpasses due to lower Sun. Sub-area dependence of that tail is quite general – it can't be caused by sunglint only, although according to Hyvärinen et al. (1999) sunglint is often characterized by  $R_3 > R_1$ . More work should be done for collecting information to separate the atmospheric conditions (e.g aerosol optical thickness and cloud observation geometry) in greater detail in order to find the reason.
- Another criterion for clear pixels  $R_{21} < 0.75$  is less useful. Generally, it performs usefully over Arctic in case of underlying ice-free ocean (on average over  $C$  and  $D$ ). But sometimes, it can totally bewilder an analyser (in the station reported almost clear cases over  $E$ ). Over snow and ice it usually gives a close ratio to that from clouds and is, therefore, useless for cloud detection.

## 5.1 The importance of $R_{31}$ for cloud mask determination

Results of Table 7 encourage us to carry out more determined numerical experiments. Separating the pixels satisfying a stronger condition  $R_{31} < \alpha$ , where  $\alpha < 0.3$ , from the area we can determine another clear area. The extent of overlapping new and old (i.e CM-SAF determined) clear areas is a measure of usefulness of the ratio for extracting cloud-free pixels in respect to the CM-SAF scheme. Larger overlapping means higher (independent) value of the ratio for that task. On the contrary, the amount of pixels, having  $R_{31} < \alpha$  but not clear according to the CM-SAF estimates the risk of using the ratio condition only. In the current situation CM-SAF results should be initially considered as true ones. Extensive comparisons with (quasi) independent features can only reveal any suspicious performance of the scheme.

Table 8: Size distribution of the common part  $\omega$  (%) of CM-SAF and  $R_{31} < 0.12$  defined clear areas

overlapping	<i>A</i>	<i>B</i> <sub>1</sub>	<i>B</i> <sub>2</sub>	<i>C</i>	<i>D</i>	<i>E</i> <sup>*</sup>
> 90%	2	1	-	-	-	-
80 < $\omega$ < 90	3	2	2	1	-	1
70 < $\omega$ < 80	-	3	3	-	4	2
60 < $\omega$ < 70	3	3	4	3	1	1
50 < $\omega$ < 60	1	6	3	4	-	4
40 < $\omega$ < 50	1	5	2	6	2	11
30 < $\omega$ < 40	4	5	5	6	-	11
20 < $\omega$ < 30	7	2	5	7	1	11
10 < $\omega$ < 20	11	8	5	5	10	2
0 < $\omega$ < 10	6	7	5	6	-	1
0	5	1	-	-	1	1

Experimental sets of clear pixels are extracted over the ARC1KM area (for all available orbits and sub-areas) using two  $\alpha$  values 0.12 and 0.08. The first value is close to the one which can be calculated from mutual threshold condition for clear, determined by Key (2002):  $R_3 < 0.04$  and  $R_1 < 0.35$  if solar zenith angle (SZA) is less than 60 degrees. Using the ratio should reduce the SZA dependence somewhat. In the present report we do not study  $R_{31}$  dependence on SZA. Later, similar extraction has been performed over the ARC1KM\_EAST area (labelled as *E* hereafter). Our first goal is to estimate the extent of clear area distinguishable by that single condition (measured by means of the overlapping part with the CM-SAF defined cloud-free area). The frequency distribution of that part for  $\alpha = 0.12$  is shown in Table 8. *E*<sup>\*</sup> on the last column means that from that sub-area only the part non-overlapping with *C* and *B* sub-areas is taken into account. Last row of the table shows the number of scenes where the condition was unable to extract any pixel. Such situations occurred in 8 cases for that sample. The scenes were very cloudy also for CM-SAF, which found not more than a few thousand cloud-free pixels maximally (see also section 7.4).

Table 8 shows that the condition  $R_{31} < 0.12$  is very strong in comparison with the whole set of CM-SAF clear/cloud-contaminated thresholds. Only for a few scenes most of the clear pixels can be found using that condition only. Generally, it can locate less than half of the CM-SAF declared cloud-free area (in case of 135 scenes from 170). But simultaneously, the condition performs usefully due to very low amount of pixels misidentified clear in respect to the main scheme (not shown in the table). Approximately half of the scenes present the best situation: all pixels declared cloud-free by  $R_{31} < 0.12$  appear to be clear also according to the CM-SAF scheme. For another half the misinterpretation part is generally less than 1% of the clear pixels. Only for 5 scenes it is higher, reaching maximum 4.2% in July 7 over *B*<sub>1</sub> area. The whole sub-area appears to be half cloud-free according to CM-SAF. Such a low per cent of misinterpretation enables us to use  $R_{31}$  in future testing.

## 5.2 Bias between T4 for clear pixels and NWP surface temperature

Previous sections show that an appropriate condition on  $R_{31}$  can distinguish clear pixels with a high confidence. T4 values over these pixels enable us a direct comparison of AVHRR/3 CH4 brightness temperature values with NWP produced surface temperature data. Such a comparison may help to estimate the performance of the cloud detection scheme which uses NWP forecasted surface temperatures for producing clear/cloud thresholds. Unfortunately, the answer cannot be unique: remarkable difference between the temperature values may be due to both errors in NWP data or wrong cloud mask detection by the method. To compare the bias  $dT = T_s - T4$ , where  $T_s$  stands for the NWP surface temperature is calculated for every pixel where  $R_{31} < 0.12$ . The bias values are averaged over all scenes and areas separately. The results are presented in Table 9.

Table 9 shows, that almost half of the scenes (82 from 170) show small bias to one side (less than 1K). Remarkably better coincidence takes place over the areas situated closer to Eurasia (i.e *B*<sub>1</sub>, *B*<sub>2</sub> and *C*). Higher quality of the NWP temperatures due to better NWP initialisation from observations, may be the reason. Near the North Pole (area *A*), the NWP temperatures show considerably warmer surfaces than can be expected by T4 data. Since the  $R_{31}$  feature appears to work quite well over the *A* area and the amount of water vapour in the Arctic atmosphere is too low to cause more than 3 K shifts, the reason should be low accuracy of the NWP surface temperature data.

Table 9: Frequency distribution of the mean temperature shift  $d\bar{T} = T_s - T4$  over different sub-areas

area	A	B <sub>1</sub>	B <sub>2</sub>	C	D
No of scenes	38	42	34	38	18
$d\bar{T} < -3$	-	-	-	-	1
$-3 < d\bar{T} < -2$	-	-	-	1	2
$-2 < d\bar{T} < -1$	1	-	-	6	6
$-1 < d\bar{T} < 0$	2	8	14	12	2
$0 < d\bar{T} < 1$	8	17	12	7	-
$1 < d\bar{T} < 2$	4	10	4	5	2
$2 < d\bar{T} < 3$	6	5	3	2	1
$3 < d\bar{T} < 4$	5	1	1	2	1
$4 < d\bar{T} < 5$	7	-	-	1	3
$5 < d\bar{T} < 6$	3	-	-	-	-
$6 < d\bar{T} < 7$	2	1	-	-	-
$7 < d\bar{T} < 8$	-	-	-	1	-

Table 10: Mean bias  $\bar{x}$  between CM-SAF thresholds and by  $R_{31} < 0.12$  defined clear area T4

Sub-area	clear % by $R_{31}$	$n_{water}$	$\bar{x}$	$n_{ice}$	$\bar{x}$
A	44.7	538690	-0.346	71190	-0.830
B <sub>1</sub>	60.0	974511	-0.424	1094732	-0.585
B <sub>2</sub>	59.3	849557	1.061	343411	-0.047
C	45.3	816775	1.421	210658	0.664
D	74.0	199380	2.314	406447	1.297

### 5.3 On the possibility of setting an automatic threshold for T4

The condition  $R_{31} < \alpha$  with a suitable  $\alpha$  value enables us to extract a group of clear pixels with a high level of confidence. T4 values for these pixels can help in getting independent (from NWP-data) estimates of the clear/cloud contaminated threshold for the pixels. The setting task likely depends on the surface type – water or snow/ice. CM-SAF saves  $T_s$  and t4 files, where the first is surface temperature (by means of NWP data) and the other the corresponding threshold increment value for CH4 brightness temperature so that  $T_s + t4$  defines the clear/cloud contaminated threshold for every pixel. Assuming we can extract clear pixels by a suitable condition for  $R_{31}$ , the variable

$$x = T4 - (T_s + t4) \quad (1)$$

calculated for these pixels can be a useful tool for testing the method. Theoretically,  $x > 0$  should hold for the main part of the clear pixels (clear pixel radiance is expected to be higher than the corresponding threshold).

$x$  values were calculated for the files considering the inner Arctic region which show larger clear areas distinguishable by means of the criterion  $R_{31} < 0.12$  (Table 8). Mean and standard deviation for  $x$  were calculated separating the CM-SAF determined surface into water and ice categories for the sub-areas A, ..., D. Part of the CM-SAF clear area, restored by the  $R_{31}$  criterion, amount of tested pixels for water and ice surface and the mean bias  $\bar{x}$  values for water and ice, respectively, are shown in Table 10.

Table 10 shows some interesting features. For all night overpasses  $\bar{x} < 0$ , showing that mean mass of newly defined clear pixels are actually colder than CM-SAF defined threshold level, meaning that other threshold tests than  $T_s + t4$  have been valid for defining the clear status. (If a strong near surface temperature inversion had been forecasted, the value of t4 would have been adjusted i.e. increased. Apparently, this did not occur which indicates that forecasted inversions (if made) were not sufficiently strong.) The situation changes totally during morning overpasses. It can be seen comparing the corresponding biases over B<sub>1</sub> and B<sub>2</sub> sub-areas. One (speculative) reason may be that HIRLAM does underestimate the daily cycle during the polar day. There is also a remarkable dependence of the biases on the underlying surface.  $x$  values over ice are always less than those

Table 11: Mean bias  $\bar{x}$  and standard deviation for  $R_{31} < 0.12$  defined clear pixels over  $E$  sub-area water, ice and land/ice

Date	GMT	CM-SAF clear	$R_{31}$ clear %	errors %	$\bar{x}_w$	$\bar{x}_i$	$\bar{x}_{l/i}$
6.07	2.15	537163	86.2	0.9	1.80±1.13	0.99±1.14	-1.01±1.55
14.07	9.17	358774	55.6	0.1	3.58±2.28	2.07±1.95	-5.74±2.06
6.08	8.37	398571	44.9	0.05	2.10±2.69	0.87±1.14	-4.91±2.71
9.08	3.00	284283	48.6	0.2	1.54±2.19	0.03±0.79	-2.90±1.48
10.08	7.54	816892	45.6	0.2	2.70±1.65	0.45±1.52	-4.78±3.19
15.08	3.38	565557	57.3	0.07	2.63±1.52	2.60±1.82	-0.36±1.48
20.08	7.50	440078	33.9	0.00	2.40±0.94	1.42±0.91	0.18±1.37
23.08	3.55	355738	27.1	0.00	1.21±0.96	0.29±1.30	-3.80±1.30
25.08	8.39	765351	59.2	0.00	4.04±1.53	2.29±1.95	-3.45±3.37
26.08	8.28	873240	64.9	0.00	3.36±1.97	1.73±1.39	-2.51±2.27
27.08	8.17	517492	49.5	0.6	3.32±2.33	2.66±1.38	-3.26±3.12

over water. Standard deviation for  $x$ , calculated for separate files (sub-area for a single overpass) is generally less than 1 K (over  $A$  and  $B_1$ ) or 2 K (for 3 other sub-areas). Frequency distributions for  $x$  are mainly asymmetric with longer negative tail (probably due to navigation errors - thresholds are calculated from a smooth temperature field, but the measured T4 values may have large deviations towards lower values). Small standard deviation for  $x$  means that the main mass of the  $R_{31}$  defined clear pixels have measured T4 values very close to CM-SAF clear/cloud contaminated threshold. This is another (indirect) verification that the method performs well over the inner Arctic region.

Results in Table 10 show area dependent behaviour for the averaged  $x$  values. Such a behaviour may lead to considerable errors in cloud monitoring due to actual bias of T4 in relation to a pre-calculated threshold field. Results of similar calculations over  $E$  sub-area (see Table 11) are very close to those for the ARC1KM area. The ARC1KM-EAST area contains several islands which are largely ice-covered. The CM-SAF scheme uses a land mask to separate water and land pixels and presents the clear pixels in four categories: land, water, ice contaminated land, ice-contaminated water. Three categories are used to study mean  $x$  values over different surface types: water, sea/ice and land+land/ice. Table 11 shows the extent of  $R_{31}$  defined clear area in comparison of CM-SAF clear, erroneously determined part, and mean and standard deviation for  $x$  over 11 more clear orbits over  $E$ . It is remarkable, that the part of misinterpretations (i.e the pixels which have  $R_{31} < 0.12$  but are at least cloud contaminated by CM-SAF) is less than 1% for all cases. On the same time, the condition extracted from 27 to 86 per cent of the CM-SAF clear area. Temperature deviations for  $E$  area are largely similar to those for sub-areas  $C$  and  $D$ .

In order to study whether  $x$  values behave independently over different surface types or have some common course individual results for every orbit are shown in Fig. 7. The orbit numeration on horizontal axis is consecutive.  $x$  values for mean clear are calculated using CM-SAF clear categories 1 – 4 over  $E$  sub-area. Separation according to water, ice and land/ice is produced only using  $R_{31}$  defined clear areas. Such a restriction has been used in order to reveal any possible by-effect of that condition.

Fig. 7 shows that the mean  $x$  values for all clear area are fluctuating mainly above zero level. This is as expected: a clear pixel T4 is generally higher than the corresponding threshold. The closest curve to the mean one is that for sea/ice category. Temperature difference over water surface is almost every day positive and over land/ice regions clearly negative. Fluctuations of  $x$  over different surfaces can be divided into two groups: harmonious or independent. In the first case one possible reason might be in biased NWP surface temperature data over the whole area. We shall return to that case in Conclusions. In the other case the possible explanation is more difficult. Some fluctuation is certainly caused by considerable variability in the extent of different clear areas. Generally, land/ice clear category has much lower extent than that for water or sea/ice and might be smoothed out by the NWP models 44 km grid resolution.

#### 5.4 Sensitive threshold for dT45

Inoue (1987) introduced the feature dT45 as a useful tool for cloud detection (mainly thin cirrus) due to different emissivity of ice clouds in these wavelengths. Water clouds are black (from thickness of

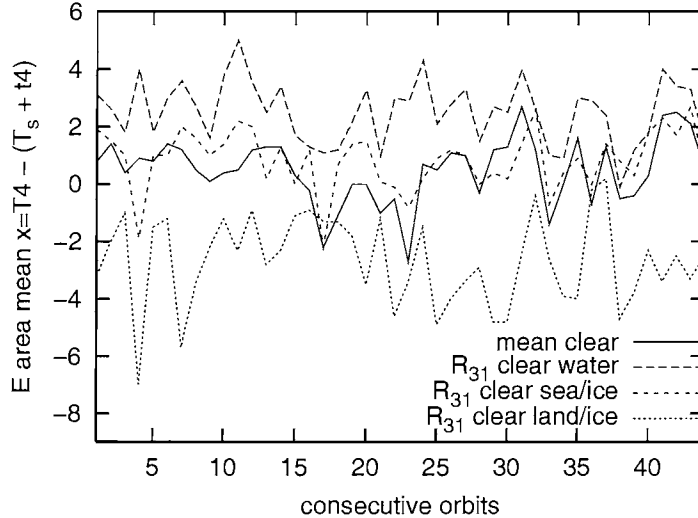


Figure 7: Comparison of orbital  $x$  values for CM-SAF clear and  $R_{31}$  defined clear water, sea/ice and land/ice areas

about 500 m) for these wavelengths and thus their  $dT_{45}$  is close to zero (e.g Stephens 1978).

Useful threshold  $t_{45}$  values for  $dT_{45}$  depend on water vapor, scanning angle and temperature. CM-SAF uses gridded NWP temperature and water vapor data together with satellite zenith angle information to precalculate  $t_{45}$  values for every pixel. The most remarkable thresholding errors may occur if the NWP temperature and/or water vapor amount is biased (see previous subsection). Expected temperature dependence for  $t_{45}$  is nonlinear in the vicinity of 270 K (Stowe et al 1999 fig. 1) which is a very important temperature region in the Arctic during summer, and biased temperature data can lead to an erroneous cloud mask. Next follows a short description of steps used by various scientists to determine the  $t_{45}$  values for their tasks.

Stowe et al (1999) determined  $t_{45}$  values as functions of  $T_4$  by means of extensive radiative transfer calculations. They used 1200 globally distributed cloud-free atmospheric soundings in a radiative transfer model to generate a simulation database of calculated  $T_4$  and  $T_5$  for three satellite zenith angles (0, 30 and 60 degrees). These values were then used to find the  $t_{45}$  curves (for land and ocean) by fitting four or fifth-degree polynomials in  $T_4$  to the maximum values of  $dT_{45}$  for these cloud-free conditions. Their goal was choosing the  $t_{45}$  to unequivocally indicate the presence of cloud. Thus they defined the threshold as the maximum  $dT_{45}$  value that is attributable for water vapor alone. Murata and Yamanuchi (1997) obtained a close value for that threshold (0.6K) as a result of cloud studies over East Antarctica.

Exactly the same methodology as Stowe et al (1999) was used for producing the CM-SAF algorithm. It is based on the TIGR radiosonde dataset (about 3000 globally distributed soundings). This means, that the functional form of the dependence of the threshold on temperature, water vapor amount and VZA does not differ essentially in these two schemes. The crucial difference is in using the water vapor information – Stowe et al (1999) have no really measured data, CM-SAF uses NWP forecast values for every pixel.

Key (2002) uses remarkably higher values for the  $t_{45}$  in comparison with that by Stowe et al (1999). His scanning angle dependence is that from Yamanouchi et al. (1987). The highest  $t_{45}$  values for the Arctic region is obtained by Minnis et al.(2001)  $1.5 \pm 0.3$  K for the FIRE ACE region during summer months (May, June, July).

The temperature dependence of  $t_{45}$  according to Stowe et al. (1999) and Key (2002) (nadir case only) over the most important  $T_4$  interval for summertime Arctic is shown in Fig 8.

Dependence on temperature and scanning zenith angle (VZA) can be computed easily for presenting the threshold curves like in Figure 8. But their value for actual cloud detection is still unknown due to lack of reliable method of extracting atmospheric water vapor from satellite data. In order to describe the variability due to varying water vapor, CM-SAF calculated mean  $t_{45}$  values for clear pixels over the sub-areas were collected. They cover quite randomly the interval from 0.7 to 1.5 K (not shown). Arranging them according to actual  $T_4$  values (although they are precalculated using NWP surface temperature gridded dataset) does not reveal any temperature dependence. The reason

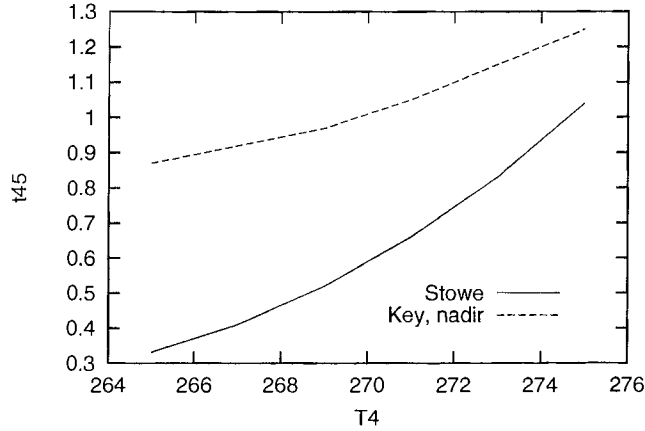


Figure 8: Threshold values  $t_{45}$  for thin cirrus test used by Stowe (1999) and Key (2002) as functions of  $T_4$

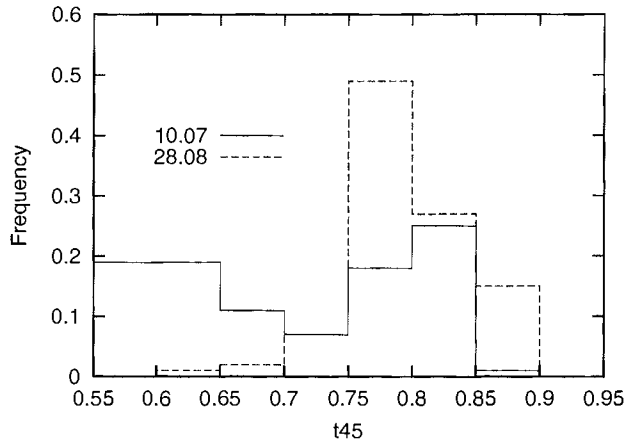


Figure 9: Frequency distribution for CM-SAF calculated  $t_{45}$  in two days in case of NWP surface temperature from 272 to 274 K and for near-nadir conditions ( $VZA < 15^\circ$ )

can be explained using table 10. It shows that most clear pixels in sub-areas  $A$  and  $B$  are colder than the precalculated thresholds. This means that also  $t_{45}$  values for these sub-areas are calculated using warmer temperature values. As a result the NWP proposed temperature dependence caused somewhat biased  $t_{45}$  values for sub-areas  $A$  and  $B$  in comparison with those which would be calculated on the basis of clear pixel  $T_4$  values.

Comparison of the produced threshold values for thin cirrus detection confirms that the thin cirrus test is the most controversial one in the schemes using AVHRR measurements. The variability range for actual  $dT_{45}$  is small, but for the threshold value, *vice versa* comparatively wide. As an example near nadir ( $VZA < 15^\circ$ ) values for  $t_{45}$  calculated by CM-SAF cloud scheme for two days (10.07 and 28.08) are shown in Fig. 9. Only the values corresponding to the NWP surface temperature from 272 to 274 K are chosen. The figure shows variability range for  $t_{45}$  caused by variations in water vapor amount during those days over the area which was situated near the sub-satellite pixels.

Comparison of the CM-SAF threshold values in Fig. 9 with curves in Fig. 8 shows that attempts in the threshold calculations to confine to average water vapor data may not be well justified (neglecting the possible uncertainty in NWP water vapor fields, which is a problem outside of our opportunities). Water vapor dependent CM-SAF thresholds get generally room in between the presented two curves. Using values from Stowe et al. (1999) many clear pixels would be defined cloudy and *vice versa*, according to the thresholds by Key (2002) a considerable amount of thin cirrus contaminated pixels would be defined cloud-free. The practical sense of that uncertainty is later considered in connection with cloud type comparison.

Table 12: Water/ice separation by a combined  $R_{31} + r06$  test (column 2) and percentage of consistency with the CM-SAF determined surface types

sub-area	surface	n	water (%)	ice (%)	other (%)	$R_{21} < 0.75$ (%)
<i>A</i>	water	227350	95.7	4.3	-	35
<i>A</i>	ice	485299	19.8	80.1	0.1	52.6
<i>B</i> <sub>1</sub>	water	64905	82.0	18.0	-	70.0
<i>B</i> <sub>1</sub>	ice	2278485	42.7	57.2	0.1	40.5
<i>B</i> <sub>2</sub>	water	326338	93.4	6.5	0.1	28.5
<i>B</i> <sub>2</sub>	ice	874745	61.3	38.2	0.5	49.3
<i>C</i>	water	770853	97.7	1.3	1.0	99.99
<i>C</i>	ice	614785	20.6	38.2	41.2	59.8
<i>D</i>	water	160349	93.3	5.5	1.2	100
<i>D</i>	ice	474789	11.4	83.9	4.7	37.6
<i>E</i> <sub>1</sub>	water	577078	67.0	30.8	2.2	86.8
<i>E</i> <sub>1</sub>	ice	451264	14.1	75.7	10.2	40.2
<i>E</i> <sub>2</sub>	water	1931375	95.5	2.6	1.9	90.0
<i>E</i> <sub>2</sub>	ice	257954	32.2	24.3	43.5	79.7

## 5.5 On the possibility to add an algorithm for water and ice separation

It has previously been shown that we can use  $R_{31}$  to define a clear data subset with a high confidence. Thus, for these pixels previously calculated threshold values ( $r06$ ) for  $R1$  may add useful information for a further separation of water and ice pixels. The  $r06$  threshold values have been computed for water surface. This means that  $r06$  for every clear pixel can be used to separate this subset into two parts. Those with  $R1 < r06$  can retain their water status, but for the others ( $R1 > r06$ ) it should be changed to ice. In order to test whether this new criterion gives similar results with CM-SAF the following separation is calculated using only the scenes with considerable number of clear pixels. For all the areas, water and ice surfaces are determined using this new approach. Simultaneously, the status by CM-SAF is determined (water, ice or something different). The results are shown in Table 12. The third column shows number of pixels for the determined surface by  $R_{31}$  and  $r06$ . Next three columns show the distribution of the same pixels according to the original scheme. Last column shows per cent of the area where  $R_{21} < 0.75$  i.e the general condition for water surface is satisfied.

Table 12 shows that the pixels where  $R_{31}$  and  $r06$  found water surface are generally obtained the same status from CM-SAF. Lowest accordance is over  $B_1$  – 82%. The results support CM-SAF used angular models to calculate  $r06$  values for ice free sea surface. Strange behaviour is exhibited by  $R_{21}$  over the same pixels. Over mostly ice free sub-areas ( $C$  and  $D$ ) the feature is in excellent accordance with the theory. In three other cases the feature is unable to distinguish between ice and water. Different illumination conditions may be one reason: average sun’s elevation is higher over  $C$  and  $D$  sub-areas.

Ice covered (or remarkably ice-contaminated) sea pixels according to  $R_{31}$  and  $r06$  obtain different status (i.e cloud free water surface) by CM-SAF. This is explained by the fact that during the development of the CM-SAF scheme the main emphasis was put on cloud detection and cloud identification rather than on the surface characterisation problem. Consequently, the snow and ice category mainly depicts surfaces with pure snow covered conditions and not pixels with more complicated content (e.g. mixed ice-water-land-snow conditions).

## 6 Detailed comparison of NOAA-14 and NOAA-16 radiance measurements

### 6.1 Difference in simultaneous brightness temperatures

The available dataset contains four cases where the time interval between NOAA-14 and NOAA-16 overpasses over the inner Arctic test areas was less than 10 minutes. The situation enables us to compare initial (remapped) satellite information for four channels over large areas. The process is important in order to properly understand cloud product differences generated by the CM-SAF scheme on the basis of different satellite data.

Table 13: Average difference NOAA-16 – NOAA-14 and its standard deviation for T4 and T5 over the common parts (all and clear pixels)

Date, area	dT44 (K)	dT55 (K)	dT4545 (K)	clear dT44	clear dT55	clear dT4545
10.07 <i>B</i>	-0.62±2.38	-0.33±2.30	-0.29±0.39			
10.07 <i>C</i>	0.09±2.83	0.29±2.80	-0.19±0.44			
11.07 <i>B</i>	-0.91±3.57	-0.57±3.52	-0.35±0.44			
11.07 <i>C</i>	-0.94±3.11	-0.65±3.08	-0.29±0.58			
11.07 <i>D</i>	0.06±2.79	0.19±2.77	-0.25±0.60			
12.07 <i>B</i>	-0.70±1.61	-0.44±1.54	-0.26±0.31			
12.07 <i>C</i>	-0.17±1.29	-0.07±1.24	-0.09±0.32			
12.07 <i>D</i>	0.08±1.05	0.26±0.97	-0.17±0.31			
13.07 <i>B</i>	-0.78±2.06	-0.60±2.07	-0.18±0.29			
13.07 <i>C</i>	-1.06±4.60	-0.74±4.41	-0.32±0.51			
10.07 <i>E</i>	-0.97±3.79	-0.75±3.75	-0.21±0.48	-1.27±2.80	-1.44±2.98	0.17±0.37
11.07 <i>E</i>	-1.18±2.90	-0.92±2.87	-0.26±0.53	-0.26±1.22	-0.35±1.24	0.09±0.24
12.07 <i>E</i>	-1.08±3.38	-0.90±3.27	-0.18±0.43	-0.12±0.88	-0.23±0.91	0.11±0.25
13.07 <i>E</i>	-1.44±3.95	-1.27±3.84	-0.17±0.51	-1.12±1.70	-1.31±1.84	0.19±0.30
6.07 <i>E</i>	0.56±3.66	0.74±3.73	-0.18±0.68	0.29±1.09	-0.44±1.20	-0.16±0.49
9.08 <i>E</i>	0.52±2.12	0.65±2.12	-0.13±0.34	0.41±0.73	0.55±0.75	-0.14±0.21
15.08 <i>E</i>	0.14±6.25	0.23±6.27	-0.10±1.00	0.26±1.82	0.27±1.92	-0.02±0.43
16.08 <i>E</i>	0.63±5.50	0.83±5.50	-0.19±0.80	0.32±1.77	0.38±1.87	-0.07±0.29

Shortwave reflectance values are not important in that stage, because the first CM-SAF cloud processing used original (not updated) CH1 and CH2 reflectance. Thus, any use of  $R_{21}$  in comparisons is not justified as soon as one component belongs to NOAA-14. Both shortwave channels updated values using July 10 2001 gain and intercept data for NOAA-14 from NASA website (<http://noaasis.noaa.gov/NOAASIS/ml/n14archive.html>), show sub-area average difference to those by NOAA-16 up to 3% for CH1 and 10% to CH2 (not shown)

Comparison of brightness temperature data for simultaneous observations over the common area is carried out as follows: for the ARC1KM area over 3 sub-areas (except *A*) and for the ARC1KM\_EAST area during simultaneous orbits. In order to get some impression about time dependence of the large scale images, the corresponding calculations between the data of those orbits which differ about half an hour are also performed.

Table 13 contains the area-averaged values for  $dT_{ii}=T_{i16} - T_{i14}$  for  $i=4,5$  together with the corresponding standard deviation values. Third column shows the difference  $dT4545=dT45_{16}-dT45_{14}$ . This column can help understanding variability in thin cirrus detection. Results are presented in three groups. Last three columns show the same characteristics computed over clear pixels. The results are presented in three groups. The first one shows the difference over the ARC1KM area for different sub-areas during four days of (almost) simultaneous observations. The second group shows the results for the large ARC1KM\_EAST area during the same orbits. Third group shows the difference for another group of days where the overpass time difference was from 24 to 35 minutes over *E* area. In order to get information about the flexibility of the CM-SAF cloud scheme the same characteristics are calculated also for the common clear pixels over *E* area.

Table 13 shows that the mean difference may be quite remarkable, almost 1 K for T4. Biases for T4 and T5 for the corresponding datasets are of the same sign keeping dT4545 comparatively low. The result is important for both cloud mask and cloud type detection, due to high sensitivity of the split window threshold  $t_{45}$  to radiation errors. It is remarkable that the mean difference in T4 and T5 for clear pixels does not differ much of that for all pixels. Standard deviation is, however, sufficiently lower for the clear part of the area. Similar relationship holds for dT4545. Mean bias may be up to 0.2 K (about the same range as that for all pixels on the presented areas). But standard deviation is remarkably lower. Biases between the brightness temperature values can easily cause bias between the determined cloud mask and cloud type. Table 13 shows that mean bias and standard deviation are varying from day to day more (e.g from 11.07 to 12.07) than from one sub-area to another. This effect is probably due to (different) navigation accuracy and different scanning angles. Even the overpasses with time difference 24 minutes (9.08 over *E*) can give better accordance in terms of both mean bias and standard deviation than the overpasses that differ 5 minutes (13.07 over the same area). There is

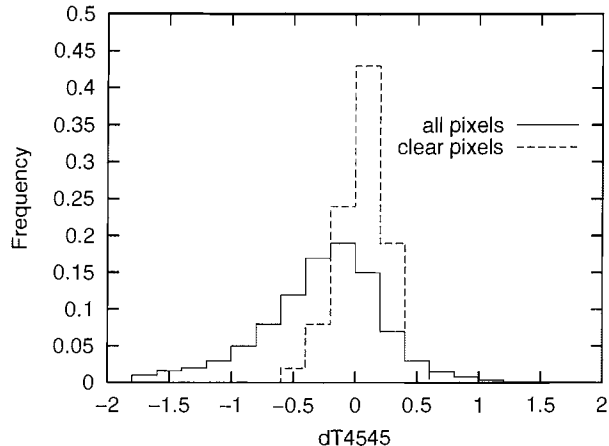


Figure 10: Frequency distribution for dT4545 over  $C$  sub-area on July 11 for all and common clear pixels

an overall tendency of producing higher dT45 values by NOAA-14 measurements. This may indicate that the amount of estimated thin cirrus is higher in NOAA-14 cloud files (the actual statistics follows).

In order to visualize the meaning of the obtained standard deviation (i.e to estimate the amount of the almost certainly differently classified pixels due to large dT4545 values) the frequency distribution for dT4545 on July 11 2001 over  $C$  sub-area is shown in Figure 10.

Figure 10 shows that if the absolute value of dT4545 is higher than 0.6 the method does not allow the pixel to have clear status by both datasets. Due to different orbits (and scanning angles) the satellites measure any pixel through a somewhat different portion of air. Thus, quite wide tails for dT4545 values (for all pixels) are not surprising.

Due to technical reasons, all of the reported difference is not caused by different radiometer versions. At least two sources should be mentioned. The first is due to the nearest neighbor approach and the other due to different viewing geometry. The effect of the latter difference might be eliminated by correctly adjusted threshold values.

## 6.2 Comparison of CH3A and CH3B performance over the common clear areas

Channels 3A and 3B play important roles in cloud detection. Thus their performance is worth a careful study. dT34 appeared historically to be a useful tool for separating clear/cloudy situations over different regions (Karlsson 1996, Kärner and Di Girolamo 2001). Initially, a simple comparison is calculated here over the common part on sub-area  $C$ . From all the pixels satisfying  $R_{31} < 0.12$  according to NOAA-16 files the condition  $dT34 < 6$  (clear according to Karlsson 1996) holds for 95% of pixels in July 10 and 86.7% in July 11. *Vice versa*, from all the pixels satisfying  $dT34 < 3$  K according to NOAA-14 files, the general guess for clear pixels  $R_{31} < 0.3$  holds for 94.5% in July 10 and 86.4 % in July 11. The 3 K limit has been chosen arbitrarily in that case. Two-dimensional frequency distributions over the four days common clear region (selected from the whole ARC1KM area) shows that 65% of clear pixels satisfy both conditions ( $R_{31} < 0.20$  and  $dT34 < 6$  K). The result indicates that the idea about finding one natural threshold for T4 (see Kärner and Di Girolamo 2001 for details) may be applicable using the variable dT34 alone on the basis of NOAA-14 observations. Cumulative results obtained from calculations over 21 orbits of NOAA-14 data are as follows: During these observations CM-SAF found 2 871 489 clear pixels and the condition  $dT34 < 3$  K 1 774 314. From the latter amount 1% was erroneously determined (treating CM-SAF decision as true). Finally, 62% of the CM-SAF clear area was distinguished by the dT34 condition. Calculating from Table 10 the corresponding value of getting clear area portion for NOAA-16 data (by means of  $R_{31} < 0.12$ ) one obtains 55.5%. This means that in relation to CM-SAF the conditions  $R_{31} < 0.12$  and  $dT34 < 3$  K are of equal power for extracting clear pixels in the Arctic. The frequency of misidentification is also similar (about 1%) in both cases. A direct comparison of the temperature shift data with Table 10 is impossible, because NOAA-14 swaths do not cover  $A$  and  $D$  sub-areas sufficiently.  $x = T4 - (T_s + t4)$  values, averaged over CM-SAF defined water and ice pixels separately, appear to be positive. This means that the

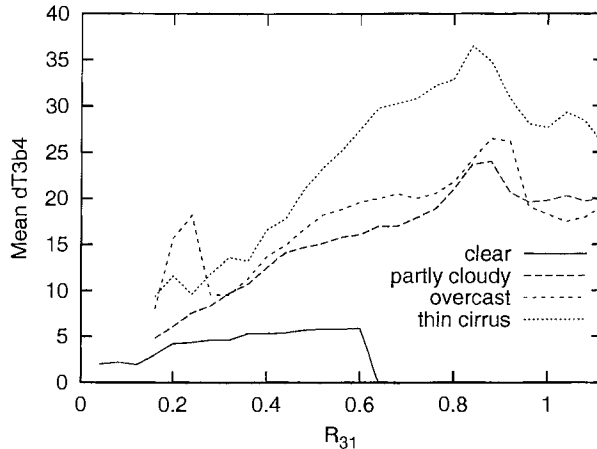


Figure 11: Dependence of the daily mean (12.07) dT34 on  $R_{31}$  calculated over common pixels of that type

accordance between NOAA-14 brightness temperature and NWP surface temperature is better than that for NOAA-16. HIRLAM temperatures for noon may be more accurate than for night or early morning. Over water  $\bar{x} = 1.52$  K and over ice 0.51 K. These results are close to NOAA-16 products for sub-areas  $B_2$  and  $C$  (it is still useful to account for general bias between T4 values from Table 13).

The previous comparison shows, that these conditions can extract clear pixels quite efficiently, with low per cent of errors. But they are unable to find all those declared clear by CM-SAF. Next, we use the conditions  $R_{31} < 0.3$  and  $dT34 < 6$  (K) to test whether one of them finds more CM-SAF clear pixels over the common part of  $E$  area during simultaneous overpasses. We treat CM-SAF clear pixels as truly clear and calculate frequency of the correspondingly satisfied conditions for about half a million pixels. The results show that the first condition is satisfied for 81.7% and the second for 83.6% of pixels. Both show clear for 72.5% and cloud contaminated for 8% of the pixels. Thus, on average, the individual value of the conditions does not differ much, although shows a little preference for dT34.

It is important to calculate the performance of dT34 over the common pixels where  $R_{31}$  is large but where the CM-SAF scheme as a whole declares a clear status. There are 17828 pixels for NOAA-16 showing  $R_{31} > 0.9$  (the value is approximately equal to the average for the main cloud types) during four simultaneous overpasses of  $E$  area. The NOAA-16 scheme decision for clear is here based mainly on the CH1 and CH4 values: these pixels are generally dark (96 % of them  $R1 < 12\%$ ) and warm (71% over the corresponding threshold for T4). NOAA-14 swaths reach 14172 of them. For the latter amount, dT34 is distributed as follows:  $dT34 < 6$  K for 36 % and  $6 < dT34 < 12$  K for 35% of the pixels. Using the condition from Trepte et al (2001), that  $dT34 > 18$  K automatically indicates the cloud contamination, only 9 % would be cloud contaminated. This comparison reveals more efficiently a significantly higher individual value of dT34 for cloud mask separation over mixed surfaces.

The interrelation between these two important features on the basis of CM-SAF determined clear partly cloudy, overcast (by opaque clouds) and thin cirrus are explained by calculating mean dT34 values for  $R_{31}$  bins of width 0.04. The results, calculated for one day (12.07) over the complete ARC1KM area are shown in Figure 11.

Figure 11 shows that there is a quite similar region of linearity between the two features over each type. This might be due to similar dependence on optical thickness of the atmosphere. The similarity disappears if  $R_{31} > 0.8$ . It is also remarkable, that dT34 values for thin cirrus (and other cirrus types which are not shown in Figure 11) are, on average, much higher than for the other cloud categories. It could mean that the thin cirrus category could be mixed up with e.g. fractional water clouds which theoretically would be capable of giving a significant contribution to the CH3B reflectance. However, since the two other cloud categories here (overcast and fractional) both include water as well as ice clouds the significance of the high dT34 values for thin cirrus is difficult to evaluate on data from one single case.

### 6.3 Which is more efficient for the cloud mask: CH3A or CH3B?

This question can have a real answer if taking the CM-SAF cloud detection scheme as a reference. Here, the answer is computed over  $E$  area using four day observations during simultaneous overpasses. The necessary frequencies are calculated over all available region (not for the common part only) for both satellites. So we have about 6 million pixels for NOAA-16 and 10 million for NOAA-14. The basic idea is simple: which of the conditions  $R_{31} < R_{cr}$  or  $dT34 < dT34_{cr}$  separates more clear pixels if the critical values change over some (disputed) region. The comparison is carried out over  $E$  area due to large overlapping of the swaths. This means that the surface conditions are mixed - water, ice, land and are not the best for  $R_{31}$ .

The relative area (in respect to CM-SAF determined total one for the corresponding type) extracted by the condition  $R_{31} \leq R_{cr}$ , where  $0.1 < R_{cr} < 1.2$  for three types (clear, opaque clouds, and semitransparent clouds) is shown in Fig. 12. The semitransparent cloud class contains types 15 and 19 in the present case (see Table 3).

Figure 12 shows that the main condition for clear over snow (i.e  $R_{31} < 0.3$ ) extracts only 58 % of the CM-SAF clear pixels over  $E$ . The value is even less than that for  $C$  (see Table 7) i.e 64%. The worst in the performance is the very slow growing rate of the extracted clear pixels with increasing  $R_{cr}$ . About 5% of cloudy or cloud contaminated pixels appear to have  $R_{31} < 0.3$ , the value slightly higher than that for cloudy pixels in Table 7 over the sub-area  $C$ .

The relative area (in respect to CM-SAF determined total one for the corresponding type) extracted by the condition  $dT34 \leq dT34_{cr}$ , where  $3 < dT34_{cr} < 36$  K for the same three types as in previous case is shown in Fig. 13.

Figure 13 shows that  $dT34 < 6$  K extract about 52% of CM-SAF clear pixels, but the number increases rapidly with increasing  $dT34_{cr}$  and reaches 90% for  $dT34_{cr} = 21$  K. The higher growing rate over the most disputable region of the corresponding feature  $R_{31}$  gives  $dT34$  some advantage in the process of cloud mask determination when both CH3A and CH3B data are available.

## 7 Detailed comparison of NOAA-14 and NOAA-16 cloud masks

### 7.1 Cloud masks during simultaneous overpasses

There are four days of observations where the time interval between NOAA-14 and NOAA-16 overpasses over the test area was less than 10 minutes. This is certainly too short time for major cloudiness changes to occur and in case of no navigation errors, the masks should coincide. Comparison of the corresponding cloud masks (1 - cloud-free; 2 - partly cloudy; 3 - cloudy; 4 - ice contaminated) over their overlapping area has been carried out. All four days were highly cloudy. The situation is unattractive over the ARC1KM area due to small part of the area to compare. Inclusion of the ARC1KM.EAST area adds the major part for the comparison. Results for four days over all sub-areas are shown in Table 14. Columns show types according to NOAA-14 and rows to NOAA-16. Main diagonal shows the per cent coinciding in both results. About 70% of the total 3.1 million pixels were simultaneously cloudy during these days. 78.5% of the types registered on the basis of NOAA-16 remain unchanged also by NOAA-14. The most remarkable change is from cloudy to partially cloudy. These occur over sub-areas  $C$  and  $D$  and where the relative azimuth angle changes to forward scattering case for the NOAA-14 scanner. For NOAA-16 the dependence on the nadir line is not registered. The NOAA-14 cloud mask results in case of backscattering mainly support the case (3) given by NOAA-16, but differ sharply across the nadir line. More detailed studies are necessary here to find the reason. Over the other sub-areas the cloud masks are in good accordance with each other.

It is worth to mention that the reason for some cloud mask (and type) difference here may be in the previously questioned quality of the NWP surface temperature and water vapor data together with viewing angle difference (see section 5.2). The brightness temperature differences may be caused by viewing angle differences for the different satellites and/or by the nearest neighbor approach which can also give different results for different satellites. But in addition to that, the actual surface temperature (approximated by  $T_4$  in case of clear pixel) may be quite far from the NWP prediction due to low resolution grid in HIRLAM. The revealed tendencies in Tables 10 and 11 showing different signs for  $T_4$  departures over water land and ice support that assumption. Empirical estimation of the differences is (generally) unable to reveal the primary purpose. A case, showing the effect of viewing angle difference will be described in a following section of cloud type comparisons.

The temperature effect can be estimated by comparing the difference between the NWP surface temperature and the CH4 brightness temperature  $dTs_4 = T_s - T_4$  for two subsets (i.e both datasets

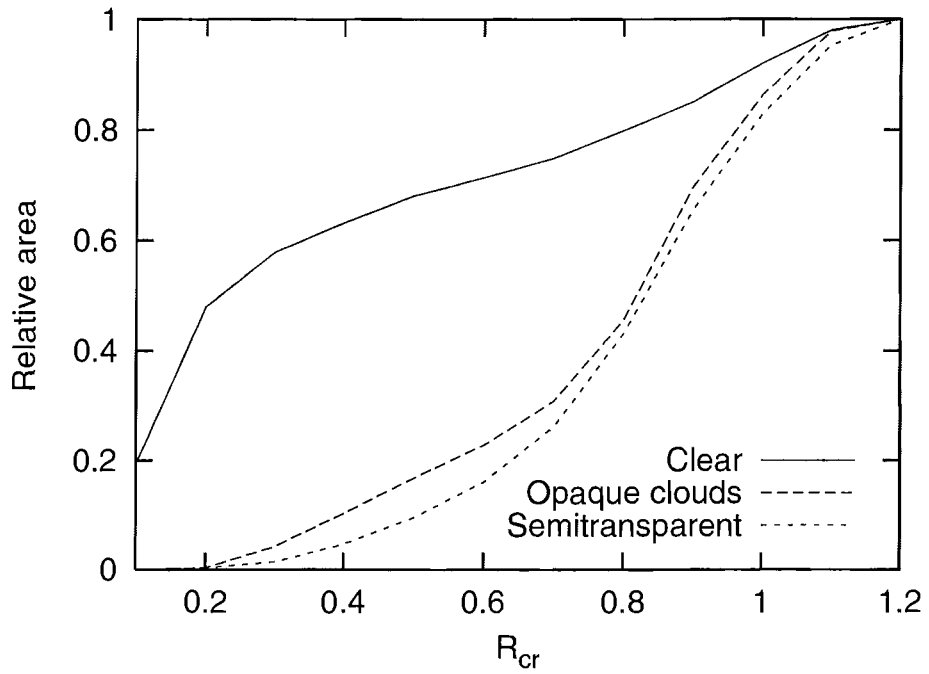


Figure 12: Area, relative to CM-SAF total for that type, extracted by  $R_{31} < R_{cr}$ , based on 4 simultaneous overpasses of the area  $E$ .

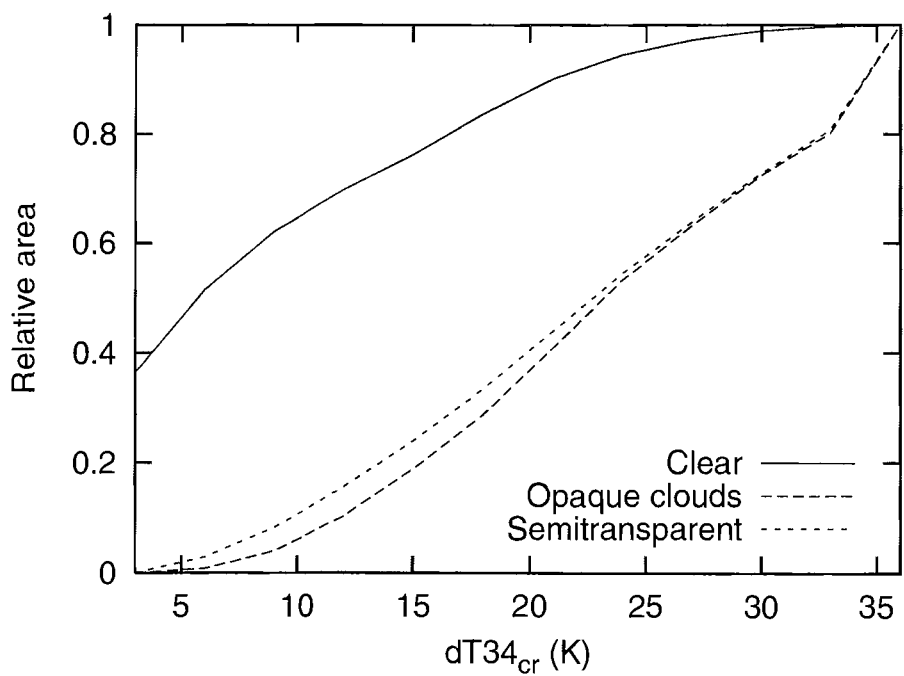


Figure 13: Area, relative to CM-SAF total for that type, extracted by  $dT34 < dT34_{cr}$ , based on 4 simultaneous overpasses of the area  $E$ .

Table 14: Comparison of NOAA-16 (rows) and NOAA-14 (columns) cloud masks (%) over all sub-areas during the simultaneous overpasses

NOAA-16 type	(1) <sub>14</sub>	(2) <sub>14</sub>	(3) <sub>14</sub>	(4) <sub>14</sub>
(1) <sub>16</sub>	7.2	0.7	1.4	0.8
(2) <sub>16</sub>	0.3	2.3	0.2	0.0
(3) <sub>16</sub>	1.2	16.1	68.2	0.6
(4) <sub>16</sub>	0.0	0.1	0.3	0.7

showing clear, correspondingly) during three days over the  $C$  area. The results show that the difference may be quite large sometimes (13.07). In this case, the difference is caused, at least to some extent, by the VZA difference (not shown). The error may (or may not) go on to the corresponding threshold values (if not compensated properly) and thus, bring about a certain bias in resulting clear parts.  $|dT_s4|$  is less than 2K in 10 and 11 July for both NOAA-16 and NOAA-14 data, but more than 4K in July 13. This case indicates that any approach (see the proposal in section 13.1) to collect independent information for estimating the available  $T_s$  data quality in pixel level is very important in order to improve the method. A 4K shift, registered on July 13, probably caused a (false) increase of partly cloudy and cloudy pixels. A very small common part of the declared clear status pixels supports that possibility (not shown). Cloud type differences for the same day are discussed later.

Cloud mask and cloud amount results are closely related. Thus, a more detailed analysis is presented in the following sections. A cloud mask comparison for other than simultaneous measurements is also carried out.

## 7.2 Taking account of partly covered pixels

How to estimate the real cloud amount for an area with partly covered pixels is one of the eternal problems in remote sensing of clouds. It is closely connected to the (quantitative) definition of clouds (how many water drops is needed to produce a contrast during the measurements). Here we'll consider the problem after any contrast (cloud contamination) is found. The amount of partially covered pixels is not small. A preliminary estimate of their frequency can be obtained using the following approximation. Let us assume, that the ground-observers field of view is equal to pixel size. In this case all the counted values from 1 to 7 octa come from partially covered pixels. Using ground based cloud cover datasets gathered up during many years, one can calculate that part. One example follows: about 40% using estimates from Matveyev (1986) over  $0.5^\circ \times 0.5^\circ$  pixels over land. These pixels are too large for comparison with 1 km resolution, but the CM-SAF determined summary frequency for types 15 and 19 over the Arctic-East area is also considerable: 24% on the basis of NOAA-16 and 28% by NOAA-14 satasnet (see Table 19). Accurate accounting for their cloud amount is an important task – errors can cause large bias. According to section 2 (Table 3, the types 16 and 17 also contain partially filled pixels. They are not included in the present analysis due to their low occurrence.

The simplest way is to follow ISCCP: all the pixels declared cloud contaminated are also treated as overcast. The approach leads to some overestimation in the produced cloud cover values (e.g Stowe et al. 1988,1989). More realistic results should be obtained using the coefficient 0.5 (so called fifty-fifty split FFS) for cloud contaminated pixels if counting for total cloud amount (Stowe et al. 1999, Mattsson and Karlsson 2002, Karlsson 2003). The approach tends to overestimate cloud amount if clouds are sparsely distributed and to underestimate it on the contrary case (Stowe et al. 1999). They proposed a scheme of calculating cloud amount taking into account cloud density in the vicinity. As a result the total cloud amount estimate for densely distributed partially cloudy pixels is higher than that for sparsely located ones (see Stowe et all 1999 for details of the estimation). One can also produce weighting schemes on the basis of temperature difference between the questionable and cloudy (or clear) pixel nearby. The corresponding scheme for clusters is applied in Kärner (2000). The approach should be easy to implement in CM-SAF due to availability of T4 values for every pixels. Only an algorithm to find nearby cloudy and clear pixels is needed in addition.

Generally, we have used the FFS approach for all cloud amount calculations in the present report. However, in sections presenting overall summary results (sections 4.4 and 7.4) the more simple method counting both cloud-filled and cloud contaminated pixels as fully cloudy has been used.

Table 15: Cloud mask and cloud amount results by both satellites over the ARC1KM area

Day	time diff.	pixels	$cm_{16}$	$cm_{14}$	$ca_{16}$	$ca_{14}$	$ca_{216}$	$ca_{214}$
07.10	9	527912	0.89	0.90	0.83	0.85	0.79	0.78
07.11	8	940530	0.91	0.90	0.80	0.83	0.79	0.78
07.12	8	890086	0.83	0.82	0.76	0.77	0.74	0.72
07.13	5	826959	0.93	0.96	0.88	0.92	0.84	0.82
07.14	215	1082193	0.83	0.86	0.73	0.79	0.69	0.72
07.16	102	1189548	0.90	0.95	0.80	0.85	0.74	0.76
07.18	209	881070	0.76	0.88	0.69	0.80	0.66	0.74
07.20	206	400537	0.82	0.84	0.70	0.75	0.67	0.70
07.23	201	782078	0.82	0.88	0.75	0.81	0.73	0.78
07.24	199	760293	0.66	0.73	0.65	0.72	0.63	0.68
07.28	193	493241	0.65	0.73	0.59	0.80	0.55	0.75
08.13	168	480292	0.95	0.97	0.85	0.89	0.77	0.79
08.17	263	803079	0.90	0.90	0.82	0.84	0.75	0.75

### 7.3 Cloud amounts over the ARC1KM and ARC1KM\_EAST areas

CM-SAF detected cloud amounts for 14 (late) morning scenes by both NOAA-16 and NOAA-14 observations are shown in Table 15. Similar results over  $E$  sub-area during 44 scenes (with time difference up to 8 hours) are shown in Table 23 of Appendix. The comparison results in this case depend essentially on time interval between the overpasses and cannot be used as tools to estimate the method's quality. Two FFS versions are presented to account for partially cloudy pixels. In the first one  $ca_{1xx}$  very thin cirrus (type 15) is considered to be cloud and FFS is applied only to type 19, in the second approach  $ca_{2xx}$  both controversial types, 15 and 19 are treated as partly covered. To get fully comparable dataset only the common area was considered in each day.

Tables 15 and 23 show that the mask by NOAA-14 is slightly larger than that by NOAA-16. The difference is largest for the second half of July 2001. Average difference is about 0.04. Generally, the difference increases with increasing time interval between the overpasses. (This interval, in minutes, is shown in the second column of both tables). One exceptionally large cloud mask difference occurs in 9.08.2001 over  $E$  area, where the time interval was only 24 minutes. The reason is in the small common part of the swaths.

Comparison of the estimated cloud amounts shows that if thin cirrus pixels are treated as cloud filled ones, cloud amounts by NOAA-14 are remarkably higher than those by NOAA-16. The difference even increases a bit in comparison of that for cloud masks (the average is about 0.05 over  $E$ ). The increase is (mainly) caused by fractional type 19. The corresponding type appeared to be more frequent for NOAA-16 observations during that period. With a coefficient 0.5 it brings about increased difference. If the type 15 is also treated as partly covered the results (in terms of areal cloud amounts) are much closer to each other (the difference 0.02 over  $E$ ). This is an encouraging result for those who are interested in calculating the radiation budget components. For that case thin cirrus has certainly somewhat lower effect than any opaque one. Both cloud data should lead to similar radiation flux estimates, on average.

### 7.4 Results from satellite-derived accumulated cloud amount statistics

Finally, as a rough description of the prevailing general cloud conditions in the Inner Arctic region during the period ranging from July 2 to August 20 2001, we may use the satellite-derived cloud mask results to compile an overall cloud frequency analysis. Figure 14 shows such a cloud frequency analysis for the ARC1KM\_EAST area. Here, the cloud frequency is simply the percentage of all the available scenes (as visualised in Fig. 2) where an individual pixel (at a fixed position) have experienced completely cloudy or cloud-contaminated conditions.

It is clear from Fig. 14 that the two months were very cloudy in the Inner Arctic Region. Cloud frequencies exceeded 80% over most parts except over land areas and near coasts. A decrease of cloudiness over land is realistic since the heated land areas would have better chances of dissolving the dominating Arctic low level cloud layers than the cold sea areas. However, it is also understood that the specific coastal scheme applied by the CM-SAF cloud algorithm suppresses cloudiness to some extent because of a more careful use of cloud thresholds for avoiding errors due to image navigation problems. In the lower half of the processing area results from the two satellites show good agreement

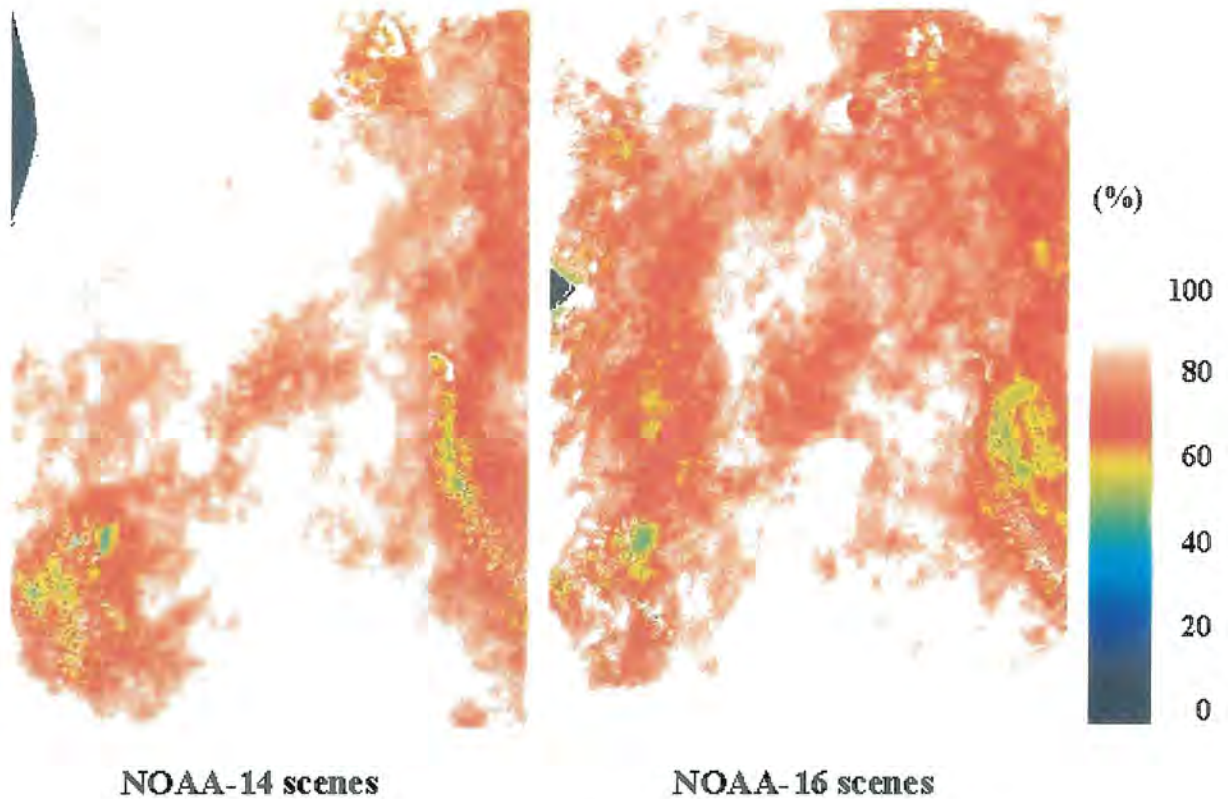


Figure 14: Cloud frequencies (%) in processing area ARC1KM.EAST estimated from all available cloud mask results in the period 2 July to 20 August 2001.

but in the upper part NOAA-14 results give higher cloud frequencies than results from NOAA-16. This difference is not likely to be a symptom of a fundamental cloud detection difference but instead a consequence of a somewhat different coverage of real satellite data for the two satellites (compare with Fig. 2). For example, in the upper half of the area the data coverage from NOAA-16 is better than for NOAA-14 and we have reason to rely more on the NOAA-16 results than on results from NOAA-14. Furthermore, many of the scenes from NOAA-16 are recorded almost 10 hours before corresponding NOAA-14 scenes which means that the existence of any diurnal (although weak) variation in cloud patterns could affect results in a similar way.

## 8 Comparison of NOAA-14 and NOAA-16 cloud types

The main cloud types found by the CM-SAF scheme on the basis of the available two month satellite measurements over the inner Arctic region are shown in Table 16 (compare with Table 3).

Cumuliform clouds were not noticed during the experiment.

### 8.1 Cloud types during simultaneous observations

Changes between these types going from NOAA-16 to NOAA-14 results are shown in Table 17. Rows show the types by NOAA-16 and columns those by NOAA-14.

According to Table 17 68% of the types have the same status by both datasets. The most remarkable systematic change, supported by the bias in dT4545 (see Table 13) over all sub-areas, is an increase of cirrus types 15 and 17 by NOAA-14 dataset. Remarkably frequent changes of all layer cloud types to fractional or subpixel cloud type and *vice versa* should be mentioned, in addition. The latter may be supported by the biases in T4 values during these days. Using not updated CH1 calibration coefficients in R3b/R1 feature may lead to increase of that bias also, but the latter influence is not considered yet. Bias in T4 (due to whichever reason) is probably responsible for some difference in the obtained opaque cloud frequencies (e.g. transition from type 7 to type 9).

Table 16: Detected cloud types and their code numbers during the experiment

Type nr	Type name
5	<i>Very low stratiform</i>
7	<i>Low stratiform</i>
9	<i>Medium level stratiform</i>
11	<i>High and opaque stratiform</i>
15	<i>Very thin cirrus</i>
17	<i>Thick cirrus</i>
18	<i>Cirrus above low or medium level cloud</i>
19	<i>Fractional or sub-pixel cloud</i>

Table 17: Changes between the main cloud types (in % of all pixels) during 4 day simultaneous observations

Type code	5 <sub>14</sub>	7 <sub>14</sub>	9 <sub>14</sub>	11 <sub>14</sub>	15 <sub>14</sub>	17 <sub>14</sub>	18 <sub>14</sub>	19 <sub>14</sub>
5 <sub>16</sub>	2.8	0.6	0.0	0.0	0.0	0.0	0.0	0.3
7 <sub>16</sub>	0.8	23.5	0.6	0.0	0.6	0.0	0.0	2.0
9 <sub>16</sub>	0.0	1.6	15.5	1.0	7.1	0.3	0.3	1.9
11 <sub>16</sub>	0.0	0.0	1.1	6.2	1.6	0.1	2.4	0.
15 <sub>16</sub>	0.0	0.1	0.6	0.2	5.4	1.4	0.2	0.4
17 <sub>16</sub>	0.0	0.0	0.0	0.0	0.2	0.5	0.0	0.0
18 <sub>16</sub>	0.0	0.0	0.0	0.2	0.4	0.1	0.7	0.0
19 <sub>16</sub>	0.4	2.5	1.8	0.0	4.5	0.1	0.0	7.3

### 8.1.1 The amount of very thin cirrus as a function of dT45

Table 17 shows that thin cirrus are more frequent according to NOAA-14 dataset than by the other. To explain possible reasons, the number of pixels satisfying the condition  $dT45 > \alpha t45$  is counted for  $\alpha = 0.8, 0.9, \dots, 1.5$  using common parts of the ARC1KM\_EAST area during four simultaneous orbit days (10.07 to 13.07). If  $\alpha=1$ , the result coincides with that by the basic scheme and all other values are normalised in respect to that. Results for both satellite data are shown in Fig. 15.

Figure 15 shows that both curves indicating the relative number of pixels are very similar. An important sensitivity estimate can be found if comparing the relative pixel number values near unity. Change 10% in relative t45 (i.e for  $\alpha$  for 1 to 0.9 or 1.1) brings about 20% change in the pixel amount satisfying that condition when comparing data from the two satellites. This is an experimental support to the statement that the dT45 bias in initial data (Table 13) might cause more cirrus clouds in NOAA-14 based products for simultaneous observations in comparison with those by NOAA-16.

Table 17 shows that a remarkable part of type (9) clouds by NOAA-16 dataset is situated in type (15) according to NOAA-14. The most expressive case is in July 11 over *E* with 133962 pixel clouds taking that transition. Thus, one solution should be wrong (or both of them remarkably biased) because radiative properties for medium level opaque clouds are clearly different from those of very thin cirrus. A 2-dimensional frequency distribution for two variables  $VZA_{16} - VZA_{14}$  and  $t45_{16} - t45_{14}$  is calculated for that scene for having more information. The results are shown in Table 18.

Table 18 shows that the transition from type 9 to type 15 occurs for pixels where VZA values for NOAA-16 is remarkably larger than those for NOAA-14. Different scanning angle produces also different threshold values by the CM-SAF preprocessing algorithm. Information in rows of the same table confirms that. All the threshold values for NOAA-16 are larger than those for NOAA-14. The reason of the transition may be due to overcompensation of the threshold values for increasing VZA. All other simultaneous orbits show the same transition, but with remarkably lower extent.

Which of the solutions might then be closest to reality? The temperature differences enable us to find the preference. Overall T4 difference for these 133962 pixels is -3.11 K. The result is logical because of the VZA difference. But the average  $T4 - T_s$  values (-17.1 for NOAA-16 and -14.0 for NOAA-14) seem to be too big for very thin cirrus. On the contrary, such a range of the temperature difference is fully acceptable in case of medium level clouds. The CM-SAF scheme for NOAA-16 reached this better solution (on average) in that case. Distribution of  $T4 - T_s$  values shows that less

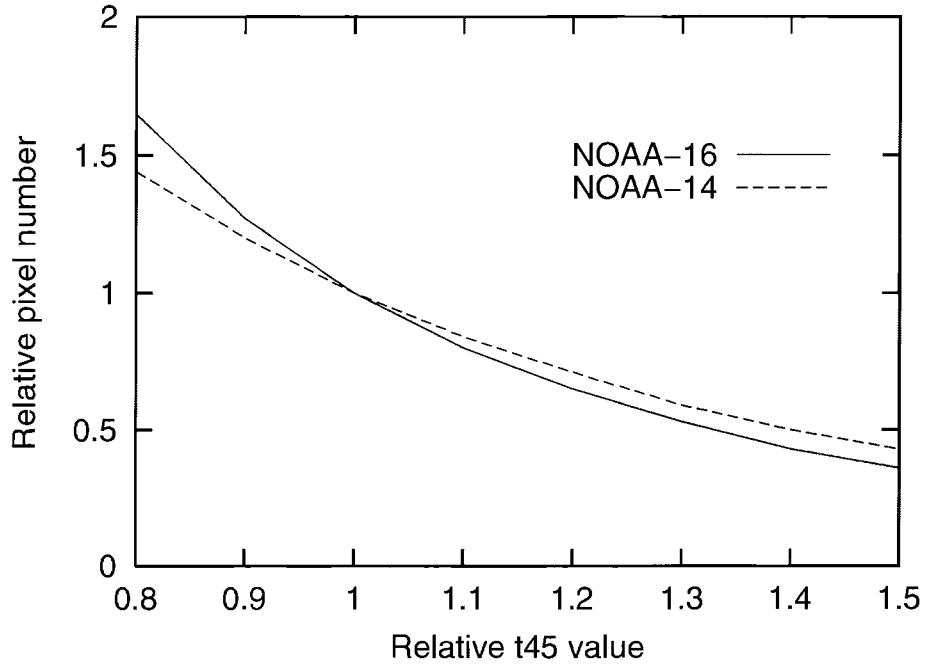


Figure 15: Relative pixel number satisfying the condition  $dT_{45} > \alpha t_{45}$  ( $0.8 < \alpha < 1.5$ ) over  $E$  area during four simultaneous orbit days (10.07 to 13.07)

Table 18: Common frequency distribution of  $VZA_{16}$ - $VZA_{14}$  (columns) and  $t_{45_{16}}$ - $t_{45_{14}}$  (rows) for the pixels which are classified to type 9 by NOAA-16 and 15 by NOAA-14

interval	0-10	10-20	20-30	30-40	40-50	50-60	60-70
0 - 0.1	0	0.003	0.013	0.024	0.011	-	-
0.1 - 0.2	-	0.002	0.005	0.031	0.008	0.004	0.01
0.2 - 0.3	-	0.033	0.038	0.054	0.028	0.019	0.006
0.3 - 0.4	-	0.052	0.045	0.063	0.043	0.019	0.006
0.4 - 0.5	-	0.005	0.056	0.026	0.051	0.017	0.002
0.5 - 0.6	-	0.009	0.058	0.020	0.040	0.002	-
0.6 - 0.7	-	0.016	0.049	0.032	0	0.003	-
0.7 - 0.8	-	0.003	0.040	0.009	-	0.006	-
0.8 - 0.9	-	0.001	0.022	0	-	0.001	-
0.9 - 1.0	-	-	0.007	-	0	0.005	-
1.0 - 1.1	-	-	0.003	-	-	-	-

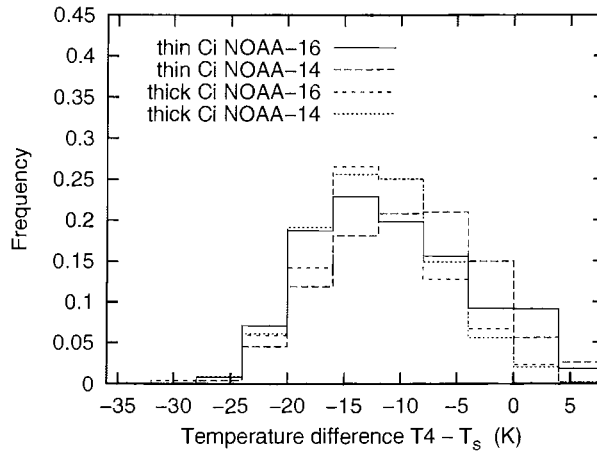


Figure 16: Frequency distributions for temperature difference  $T_4 - T_s$  for cirrus types 15 and 17 over *E* area during four simultaneous orbits(10.07 to 13.07)

than 10% of them are higher than -5 K (which might be a reasonable range for very thin cirrus). Following that, type 18 (cirrus over any lower clouds) seems to be more acceptable solution on the basis of NOAA-14 data.

### 8.1.2 Can very thin clouds have the same temperature difference with the surface as thick ones?

By the type classification, thick cirrus is opaque and thin cirrus transparent to some extent. The difference should be expressed in values of  $T_4$  over the cirrus layers. In order to test that, histograms of the temperature difference  $T_4 - T_s$  for types 15 and 17 during four simultaneous orbits are shown in Fig. 16.

Fig. 16 shows very similar distribution of  $T_4 - T_s$  for all four samples. Frequency of thick cirrus is a bit higher at the cold margin. Similarly, very thin cirrus is more frequent at the warmer margin. But the sample mean values are very close to each other (for both NOAA-14 and NOAA-16 datasets). Such a behavior seems to be in contradiction with the classification principles. More transparent type 15 should be considerably warmer on that figure. Instead of that all actual frequency curves are similarly flat and indicate large variance. Any attempt to separate the cumulative histogram of types 15 and 17 into two parts will not be an easy task. Huge overlapping remains anyway.

### 8.1.3 What is the difference between low and very low?

Two low stratiform cloud types, 5 and 7 have quite similar characteristics in terms of  $R_{31}$ ,  $dT_{34}$  and  $T_4 - T_s$ . The characteristics are calculated over the common parts during these four simultaneous orbits. According to the first 1.4 % of type 5 and 0.2 % of type 7 might be also clear (i.e  $R_{31} < 0.3$ ). Similar situation according to  $dT_{34}$  holds for 3.4 % and 1.5 % of pixels, respectively. Frequency distribution of the difference  $T_4 - T_s$  for four stratiform cloud types (5,7,9 and 11) on the basis of NOAA-16 data is shown in Fig. 17. NOAA-14 dataset does not reveal any significant difference in comparison with that.

Figure 17 shows that the distributions for type 5 and 7 are very similar. The main difference is the sign of asymmetry in respect to the mode bin. It is positive for type 7 and negative for type 5. Numerically,  $T_4$  is warmer than  $T_s$  for 29.2 % of NOAA-16 pixels (30.1 % in case of NOAA-14) for the type 5 and the corresponding amounts for type 7 are 10.2 (NOAA-16) and 22.7 (NOAA-14). The different asymmetry brings about slightly warmer mean value for type 5 sample. Other details (total range, mode bin) of the frequency distributions are more close. Similarity continues if comparing  $R_{31}$  samples. The only remarkable difference is in the situation of mode. It is in between 0.8 and 0.9 for type 7 and 0.9 and 1.0 for type 5.  $R_3$  seems to increase more rapidly than  $R_1$  in case of warmer clouds. In principle, the latter may contain more water. For  $dT_{34}$  the mode is generally situated between 16 and 24 K for both types but has remarkable variations between the four days. One intriguing question arises on the basis of Fig. 17: Maybe the water clouds with near surface temperature can be classified

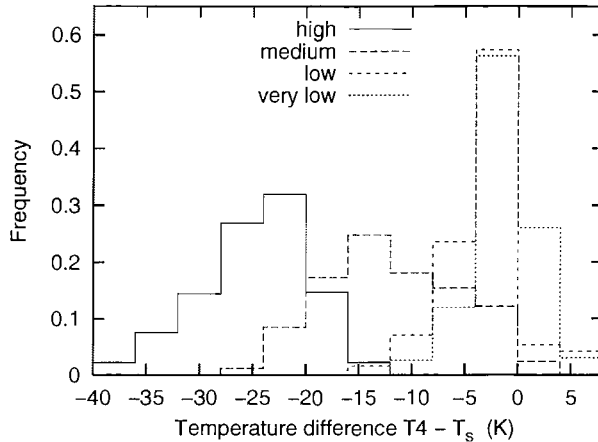


Figure 17: Frequency distributions for temperature difference  $T_4 - T_s$  for cloud types 5,7,9 and 11 over  $E$  area during four simultaneous orbits(from 10.07 to 13.07)

Table 19: Summary of main cloud type frequencies measured during the same day by two satellites over all testareas.

Type	code	NOAA-16	NOAA-14	common part
<i>Cloudfree</i>	(1 – 4)	16.3	11.7	8.7
<i>Very low stratiform</i>	(5)	4.1	4.0	2.2
<i>Low stratiform</i>	(7)	26.5	28.8	18.6
<i>Medium level stratiform</i>	(9)	20.1	18.1	10.2
<i>High opaque stratiform</i>	(11)	6.8	4.8	2.6
<i>Very thin Ci</i>	(15)	8.5	14.9	3.6
<i>Thick Ci</i>	(17)	1.2	2.4	0.5
<i>Ci above lower clouds</i>	(18)	1.1	2.3	0.3
<i>Fractional or sub-pixel clouds</i>	(19)	15.4	13.3	4.8

as one and the same type? The answer depends on their drop size distribution, optical thickness etc, and certainly, can not reached in the present report.

## 8.2 Cloud type changes during the same day

Wider comparisons are possible if allowing longer periods between the overpasses. CM-SAF cloud types detected during the same day (by means of NOAA-16 and NOAA-14 data) present large amount of cloud type results for comparison. Generally, the time interval between measurements has been less than four hours. Thus, some changes of cloud types/amounts due to natural development in cloud fields should be expected. Direct comparison of transitions between the types makes no sense because it can not characterize only the method any more. The comparison of main types obtained on the basis of two datasets and their common part is shown in Table 19.

Table 19 shows that increase in the time difference between overpass brought about some decrease of the area of the same cloud type in comparison of Table 17 – from 68% to 42.8%. Adding to that 8.7% of the common clear area (not counted in Table 17) one can conclude that CM-SAF made the same decision for half of the cases. Five most frequent groups (clear, low, medium, fractional and very thin cirrus) show also largest difference on the basis of two datasets.

## 8.3 Cloud type statistics from the complete satellite dataset

One way of getting a rough estimate of the differences between cloud type results from the two satellites is to generate cloud type statistics (cloud type frequencies) in a similar way as was done previously in section 7.4. Fig. 18, Fig. 19 and Fig. 20 show such results for the cloud categories High-level (including all high opaque and all Cirrus types), Medium-level and Low-level (including Very-low and

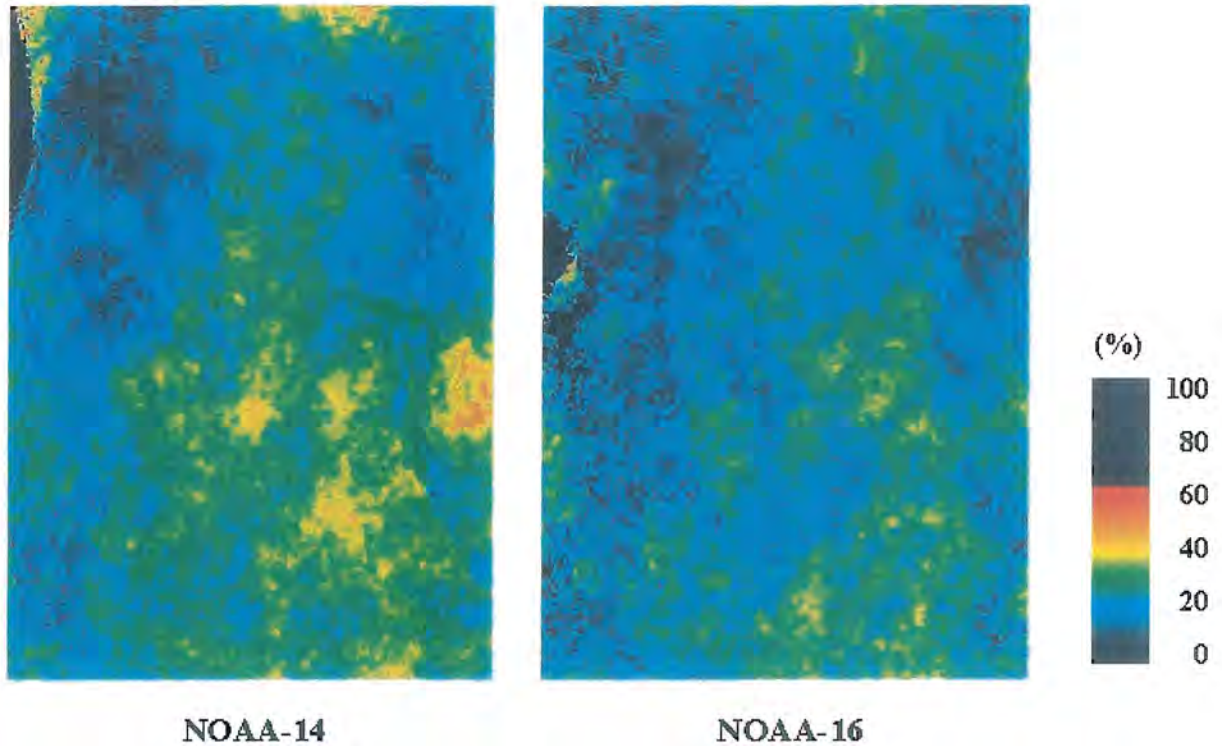


Figure 18: Contribution (%) from **HIGH-LEVEL** cloud types in processing area ARC1KM.EAST estimated from all available cloud type results in the period 2 July to 20 August 2001.

Low types) clouds (compare with listing in Tab. 19. Only the results for the High-level category could be seen as a true cloud frequency while the others are pseudo-frequencies since no information about the occurrence of these cloud categories is known when higher level clouds are present. Thus, these pseudo-frequencies for Low-level and Medium-level clouds will be lower than in reality. A summing up of all three components plus the category Fractional (not included in any of the three cloud layer categories) will yield the results previously shown in Fig. 14.

In Fig. 18 we notice that the frequency of high cloud types are high in the lower and central part of the region. The same cloud pattern is shown by both satellites but frequencies are somewhat higher for NOAA-14. This difference is not completely understood but might be due entirely to the differences in sampling and coverage. The given distribution of high-level clouds appears to be realistic when considering that most of the contribution should be given by cloud systems connected to moving extratropical cyclones along the Polar front. Since cyclone tracks near the pole are quite unusual we should expect these frontal clouds to be more frequent in the lower, central and right part of the processing region.

A similar reasoning should hold in theory also for the Medium-level clouds which are described in Fig. 19. But, as we can see here, the cloud pattern is very different from the pattern of High-level clouds. The highest frequencies are now found in the upper part of the region, quite close to the North Pole. This distribution is probably not representative for the true distribution of Medium-level clouds and the explanation is most likely that the Medium-level clouds connected to frontal clouds along the Polar front have been hidden by higher level clouds.

The contribution from Low-level clouds shown in Fig. 20 gives an occurrence exceeding 30% over most of the area. At some places, (preferably in the left portion of the area) the occurrence exceeds 50%. It is likely that the true occurrence of Low-level clouds is significantly higher than the values shown here when considering the possible occurrence also in areas with Medium-level and High-level clouds. Some indications of a mis-classification of Low-level clouds as Medium-level clouds could be seen from visual inspection of classification results. Apparently one and the same cloud layer was often transferred from Low-level types to Medium-level types when approaching areas near the Pole. This could explain the high frequencies of Medium-level clouds seen here in Fig. 19. This problem is likely to be caused by the fact that the transition from Low-level to Medium-level clouds in the CM-SAF cloud scheme is determined exclusively by a direct comparison of brightness temperatures to

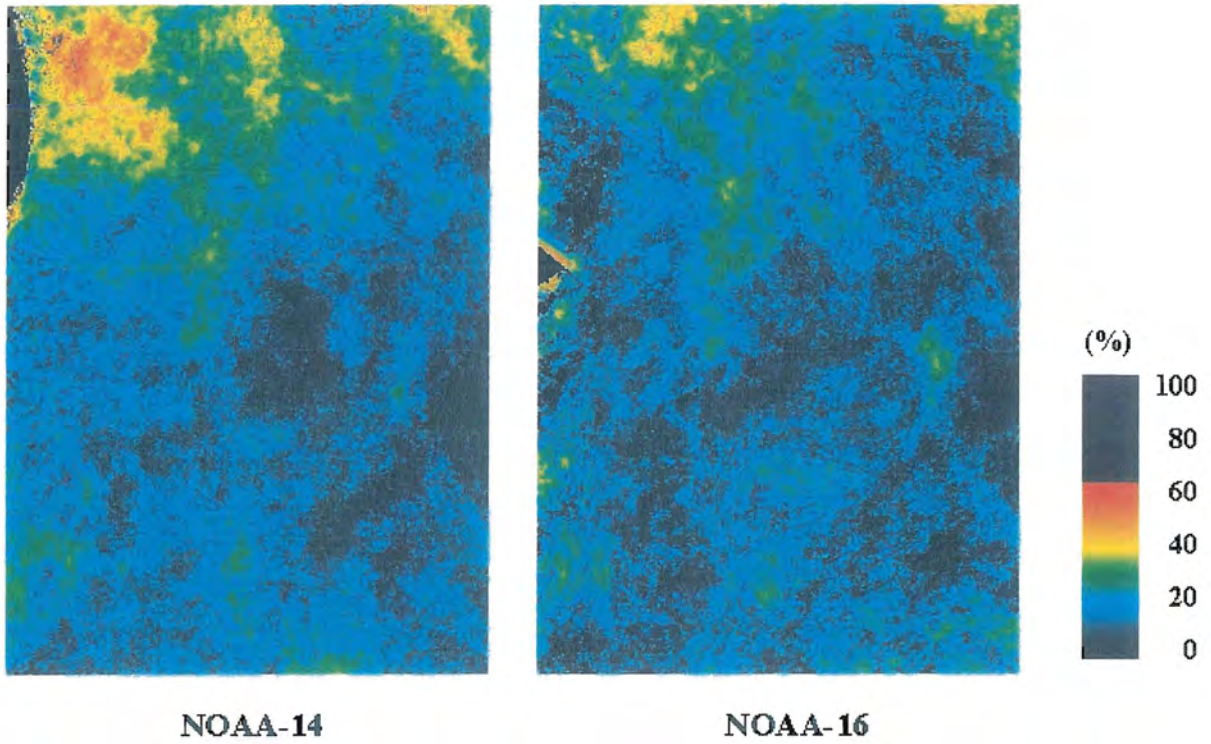


Figure 19: Contribution (%) from **MEDIUM-LEVEL** cloud types in processing area ARC1KM.EAST estimated from all available cloud type results in the period 2 July to 20 August 2001.

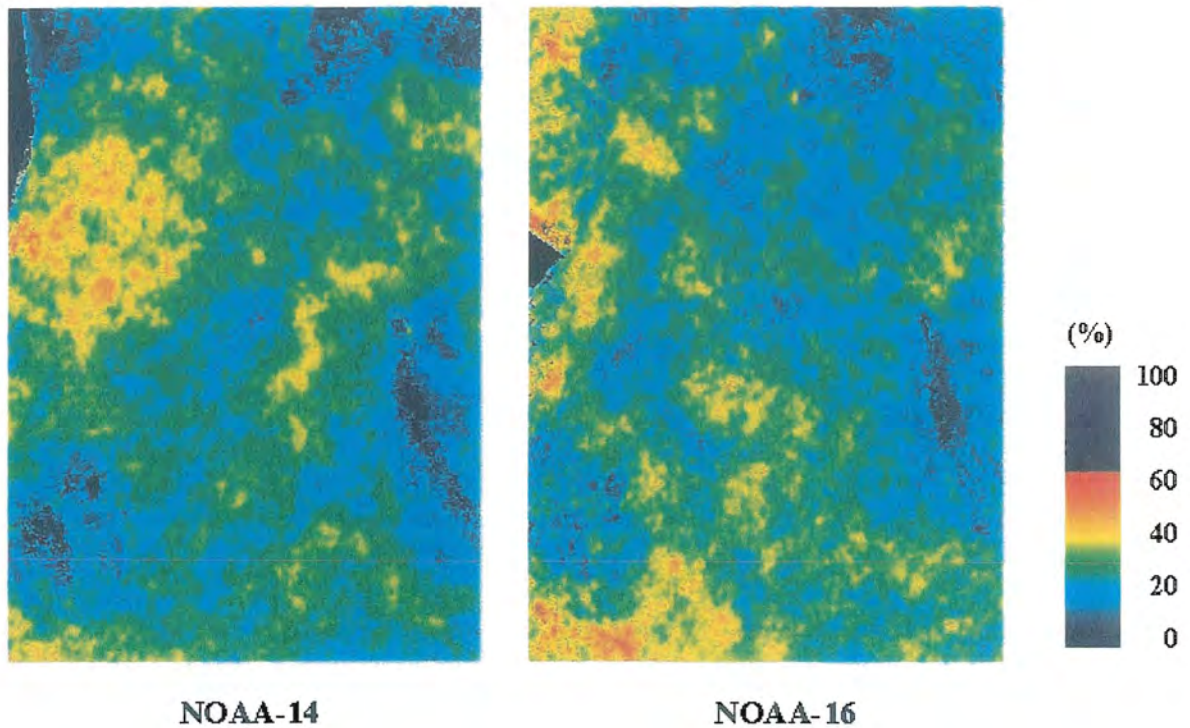


Figure 20: Contribution (%) from **LOW-LEVEL** cloud types in processing area ARC1KM.EAST estimated from all available cloud type results in the period 2 July to 20 August 2001.

Table 20: Mean and standard deviation for cloud top height (m) by NOAA-16 and the difference with NOAA-14 during simultaneous overpasses of the area  $E$ .

Date	Type	mean $H_{16}$ (m)	difference $H_{16}-H_{14}$
10.07	5	2550±1068	105±167
11.07	5	4870±369	134±124
12.07	5	4000±730	26±126
13.07	5	3556±1068	105±167
10.07	7	4558±955	42±125
11.07	7	4633±1276	75±131
12.07	7	4325±914	35±116
13.07	7	3915±1669	-27±308
10.07	9	5755±666	62±273
11.07	9	6242±1436	88±359
12.07	9	5543±1376	35±116
13.07	9	4996±951	73±270
10.07	11	7407±633	92±524
11.07	11	7888±640	20±139
12.07	11	7452±686	223±667
13.07	11	6936±893	80±612

the temperatures of the 700 hPa level from short-range NWP model forecasts. However, the 700 hPa level is generally at a lower altitude in the vicinity of the Pole compared to at other latitudes. The atmosphere is generally thinner at the pole than at other latitudes, especially compared to conditions in tropical regions. This fact could introduce an artificial transition of cloud types since it is not certain that main cloud types behave in a similar way (i.e., having the same reduction in their typical altitudes in the vicinity of the pole). It must also be said that the efficiency for satellite-based algorithms of accurately separating Low-level and Medium-level cloud types is very difficult to evaluate. The reason is that the definition here must be based on cloud-top properties while any classification made from the surface is based on cloud-base properties. Thus, a dependency on cloud thickness exists and could cause large deviations when comparing ground-based and satellite-based analyses.

Finally, even if there are differences between visualised cloud frequencies from the two satellites, it is not considered likely that this represents true performance differences. Most of the differences could be appointed to the differences in sampling frequency and coverage.

## 9 Comparison of NOAA-16 and NOAA-14 cloud top heights

### 9.1 Cloud top heights during simultaneous observations

Cloud top height results (in meters) over  $E$  area during four simultaneous overpasses are shown in Table 20. Only the common area is used in each day.

Table 20 show that cloud top heights seem to be too high. Those for types 11 and 9 are in good accordance with the midlatitude cloud heights on the basis of the textbook information. But very low (5) and low (7) cloud heights appear to be suspiciously too high according to any latitude model. Mean values and standard deviations for different days show larger variability also for types 5 and 7. Differences between NOAA-14 and NOAA-16 scheme results are reasonably low. Even the standard deviation is much lower for the difference. This means that the suspicious results are not caused by AVHRR information.

The averaged cloud top pressure results over  $E$  area, common for both satellites, during four simultaneous overpasses are shown in Table 21.

The average cloud top pressure results follow correctly those for top height. For types 9 and 11 they are realistic but for types 5 and 7, also the cloud top pressure values are highly suspicious.

Table 21: Mean and standard deviation for cloud top pressure (mb) by NOAA-16 and the difference with NOAA-14 during simultaneous overpasses of the area  $E$ .

Date	Type	mean $P_{16}$ (mb)	difference $P_{16}-P_{14}$
10.07	5	753±98	2.3±13.0
11.07	5	565±27	-9.3±12.6
12.07	5	617±42	-1.6±12.4
13.07	5	660±90	-10.9±42.5
10.07	7	590±77	-2.0±11.8
11.07	7	587±94	-5.6±12.4
12.07	7	604±67	-2.3±11.4
13.07	7	614±166	-13.6±106
10.07	9	504±44	-4.0±19.5
11.07	9	476±91	-5.2±22.5
12.07	9	523±69	-4.5±18.7
13.07	9	551±70	-4.3±19.7
10.07	11	400±35	-4.9±30.1
11.07	11	374±31	-1.1±10.1
12.07	11	400±37	-11.9±37.7
13.07	11	419±50	-4.1±36.1

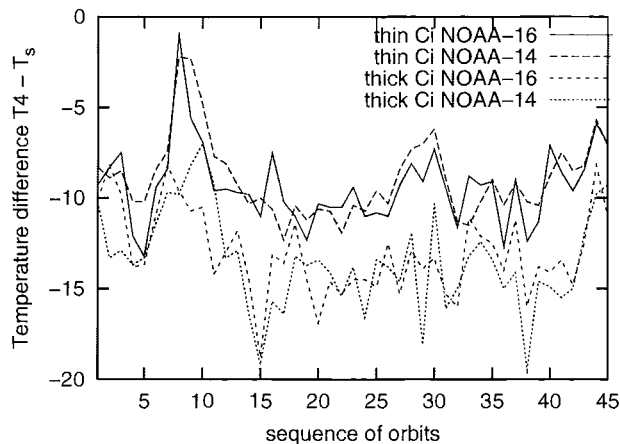


Figure 21: Time series for the area averaged temperature difference  $T_4 - T_s$  for cirrus types 15 and 17 over  $E$  area during all orbits

## 10 Characteristic time series for the main Arctic cloud types in summer 2001

Some characteristics describing radiative properties of cloud fields are calculated for all available orbits over the  $E$  area. The temperature difference  $T_4 - T_s$  is one of them. Time series for its average values during 45 orbits over the ARC1KM\_EAST area ( $E$ ) for both cirrus types are shown in Fig. 21. The general relationship between the cirrus types should be evident – very thin cirrus is always more transparent than thick one. Provided their mean height being the same, on average, the corresponding curves should be situated on different heights. They do, but is the difference value satisfactory? NOAA-16 and NOAA-14 based samples differ not much. There is an interval of very stable temperature difference between the 15 and 17 type values (second half of July 2001). Some exceptional days exist (e.g 14.07) where the average temperature difference for thin cirrus class was 1 K.

A similar temperature difference for very low and low stratiform cloud types (5 and 7, respectively) is shown in Fig. 22. The figure indicates even more difficult type separation problems. Lines between the types sometimes differ less than those between the satellites. If one had to decide on the basis of that chart only it would be difficult to term the types 5 and 7 different. Two short and strong

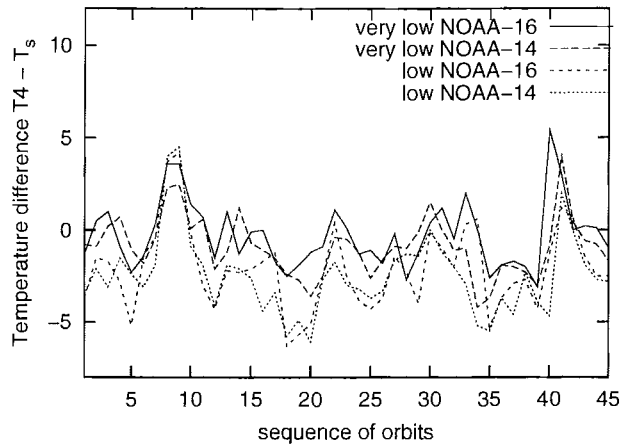


Figure 22: Time series for the area averaged temperature difference  $T_4 - T_s$  for very low and low stratiform types 5 and 7 over  $E$  area during all orbits

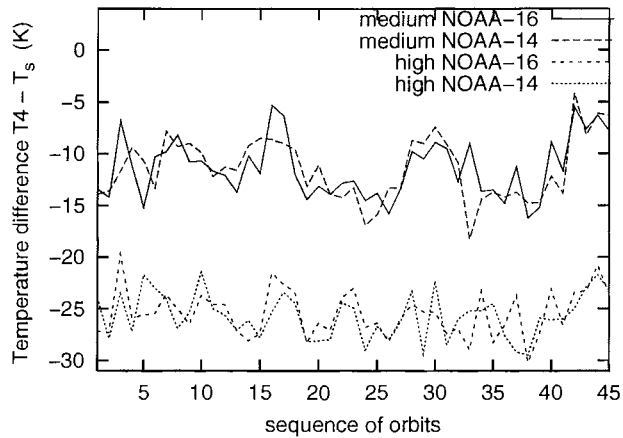


Figure 23: Time series for the area averaged temperature difference  $T_4 - T_s$  for medium 9 and high stratiform 11 cloud types over  $E$  area during all orbits

warming periods can be observed. The first one (July 14 - 15.) coincides with similar warming event in cirrus types. Another (August 23 -24.) seems to be characteristic for low clouds only.

The same temperature difference time series for medium (type 9) and high opaque stratiform (type 11) clouds are shown in Fig. 23. These cloud types are characterized by a stable average brightness temperature difference between the layers (about 10 K). One reason is certainly due to use of the same NWP based  $T_s$  and 750 and 500 mb temperatures used for the classification. Both satellite datasets show good accordance and no warming in the middle of July. But in the end of August quite a remarkable warming occurred.

Time series of the  $E$  area-averaged  $R_{31}$  for 6 main determined cloud types are shown in Fig. 24.

Time series of  $dT_{34}$  values for all 6 main Arctic cloud types are shown in Fig. 25. The parameter is strongly dependent on optical thickness of clouds and therefore differences between the types are not very systematic. Considerably large jumps ( $>10$  K) between the area mean values of consecutive orbits are generally caused by variability in optical thickness. Curves for types 17 and 11 are generally higher than the others and curves for 5 and 7 lower. A remarkable trend of decrease towards the end of summer can be observed. This may be an indication of annual course in CH3B due to changing solar elevation.

CM-SAF calculated cloud top height results (in km) are shown in two figures. Fig. 26 shows averaged over  $E$  area top height results for very low (type code 5) and low (7) cloud types.

Fig. 27 shows averaged over  $E$  area top height results for medium (9) and high (11) stratiform cloud types.

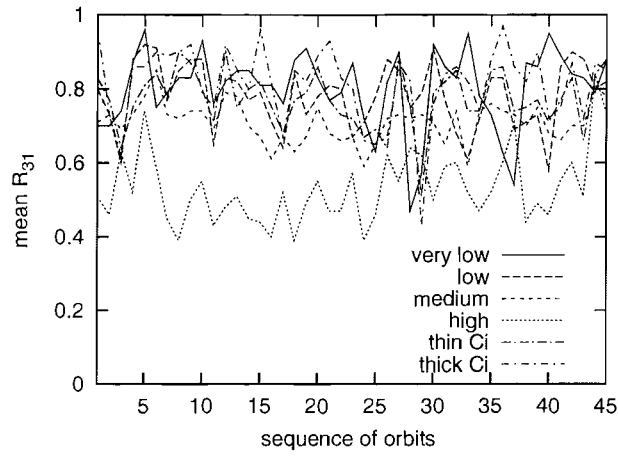


Figure 24: Time series for the area averaged  $R_{31}$  for 6 main arctic cloud types over  $E$  area during all orbits

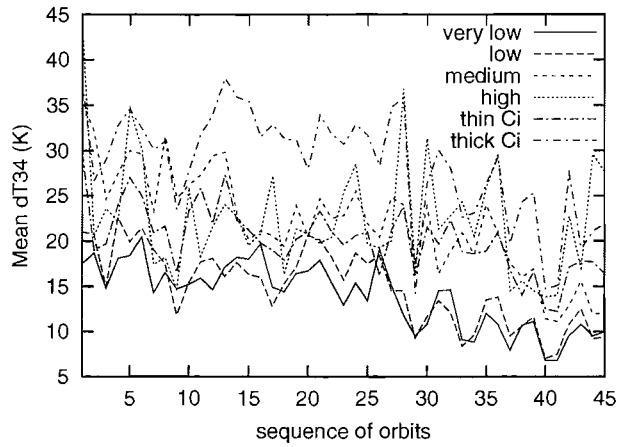


Figure 25: Time series for the area averaged difference  $dT_{34}$  for the main 6 cloud types over  $E$  area during all orbits

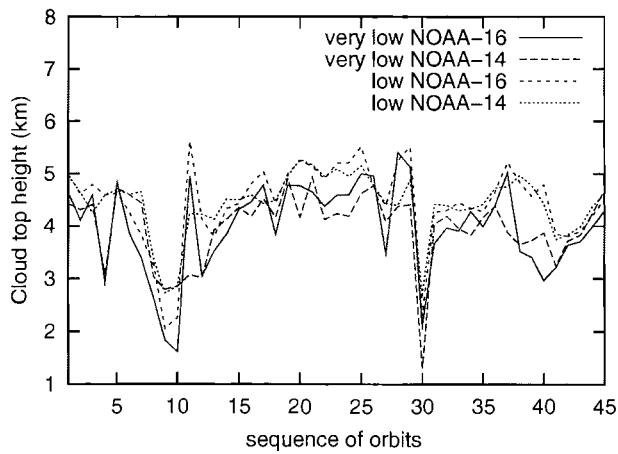


Figure 26: Time series for the  $E$  area averaged cloud top heights for very low (5) and low (7) types during all orbits

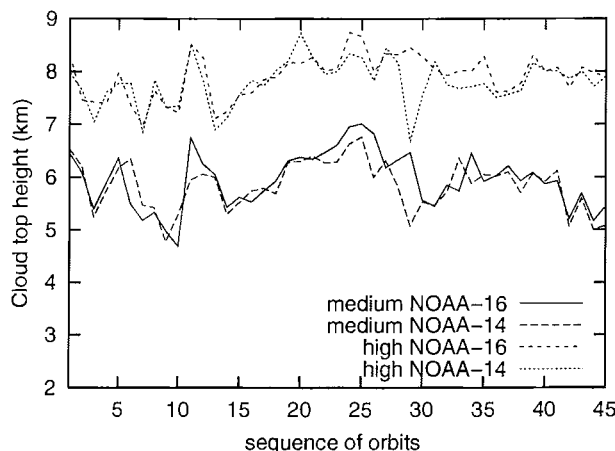


Figure 27: Time series for the *E* area averaged cloud top heights for medium (9) and high (11) types during all orbits

Cloud top height time series show similar behaviour to that observed if comparing simultaneous orbit products. The top heights for types 5 and 7 seem to be strongly overestimated (except for two or three cases). The results for medium and high opaque clouds are much more realistic.

## 11 Some solutions to encountered problems of cloudtop and cloud type products

It is obvious from the results in sections 9 and 10 that the retrieved cloud top information is completely unrealistic for the Arctic environment. The magnitude of the errors appears to be so large that a major coding error seems more likely than that the error should originate from a weakness in the applied methodology. That this actually was the case could be confirmed in a very late phase of this study. An NWP grid point mapping error was discovered which meant that temperature profiles from areas far off the Arctic region by mistake was used in the cloud top determination process.

It was not possible to redo all the cloud top calculations in sections 9 and 10 with the corrected cloud top algorithm due to time constraints. However, below in Figure 28 and Figure 29 is given one example of how results were changed after the correction of the scheme had been carried out. Changes are dramatical and the new results appear to give much more realistic results when comparing to the domination of low-level cloud types (compare also with cover picture). We hope that this correction in general will give a much more realistic description of summertime cloud altitudes in the inner Arctic region but future more detailed studies have to confirm that this is actually the case.

Worth noting here is that this NWP mapping error had avoided detection when the Cloud Top Height algorithm was originally developed in the SAFNWC project. For the error to become clearly visible it was necessary to use NWP data near the boundaries of the NWP model domain which indeed was the case for the inner Arctic Cloud Products feasibility study. In this respect this result could be considered very valuable also for the SAFNWC project.

It should also be mentioned that one weakness of the cloud type processing algorithm concerning the treatment of the cloud type category Thick Cirrus (category 17 in Table 3) has also been discovered. A missing temperature test leads here to the risk of mixing up thick cirrus clouds with fractional water clouds which have been noticed in the results. It is planned to implement a correction for this defect when it is assured that no additional negative effects are introduced.

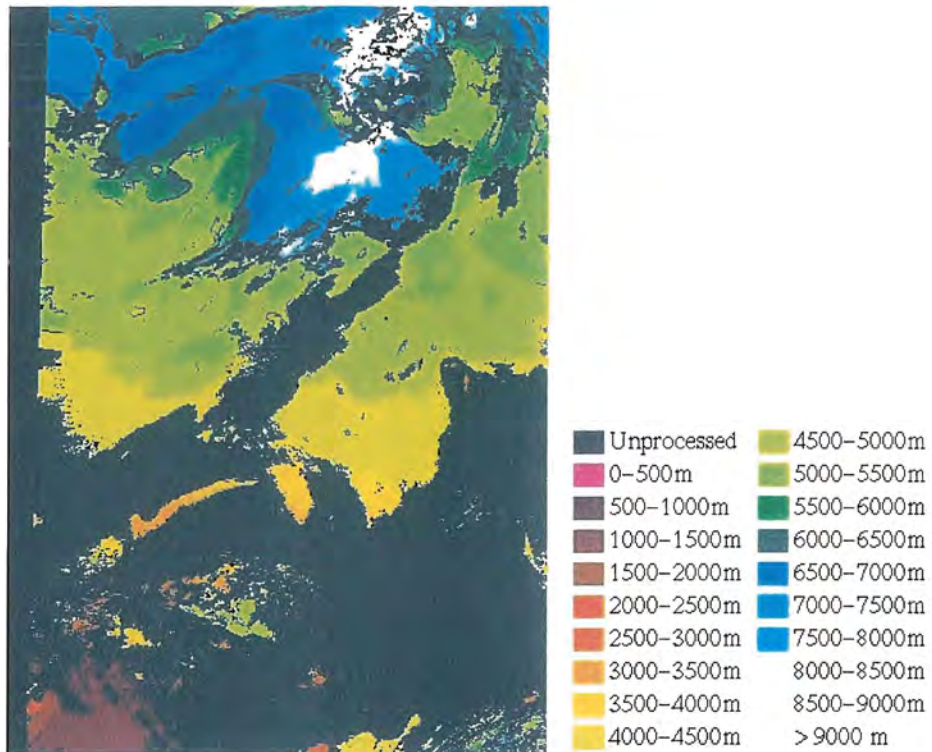


Figure 28: Original cloud top temperature product over the ARC1KM.EAST area from 8 August 2001 at 11:11 UTC.

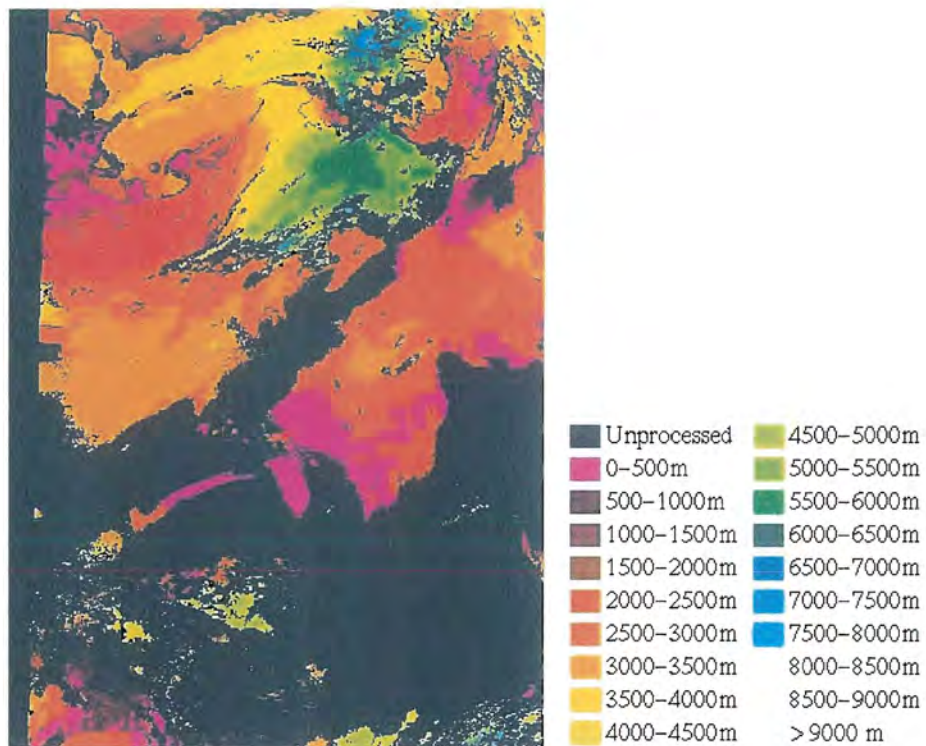


Figure 29: Revised cloud top temperature product over the ARC1KM.EAST area from 8 August 2001 at 11:11 UTC.

## 12 Maximum ice extent analyses

Since the main goal of the envisaged CM-SAF processing in the Inner Arctic region is the possibility to study potential changes in the polar sea ice albedo (see Preface section), a simple ice analysis experiment has finally been carried out based on the achieved cloud mask results. The idea has been to test if it is possible to produce analyses of the maximum ice extent during limited periods by use of cloud mask results and a simple interpretation of the information from the visible AVHRR channel 1 at 0.6 micron (image feature R1). Successful results here (compared to other available ice analyses) would indirectly support the idea of a final analysis of sea ice albedo.

The concept used here has been the following:

- Two periods were selected: 2-15 July and 1-15 August. The first period would be representative for the maximum ice extent over the studied region and the second for the minimum ice extent in the complete analysis period (2 July - 28 August 2001).
- For all cloud-free portions (as determined from cloudmask results) in the selected AVHRR scenes, pixels were re-labelled as ice-covered if being brighter than the applied cloudy threshold in feature R1. Recall that the reason for these pixels being labelled as cloud-free is that no other cloud tests in other features (required to be positive at the same time) had been passed. Thus, ideally a bright pixel in AVHRR channel 1 must then be either snow- or ice covered if not been assigned cloudy. Since we know from previous sections that a small fraction of all clouds seem to have remained undetected by the cloud mask (mainly due to shadow effects), a safety margin of 10% reflectivity have been added to the cloudy threshold in this particular analysis.
- The results for all selected AVHRR scenes in the chosen period were then accumulated to produce a maximum ice extent analysis. The maximum ice extent would then be formed by all pixels that at least one time in the period was assigned as ice covered.
- The final results were compared to SSM/I-based ice concentration analyses developed in the EU-project ARTIST - Arctic Radiation and Turbulence Interaction Study (see <http://www.awi-bremerhaven.de/ATM/ARTIST/> and Kaleschke et al, 2001).

The direct comparison of results in Fig. 30 and Fig. 31 is complicated by the fact that the ARTIST analysis covers a much larger area and is presented in a different map projection. But by the help of the visible land areas and the definition of the CM-SAF processing region ARC1KM.EAST (see Fig. 1) we can see that the agreement is very good, also in individual details.

For example, the CM-SAF analysis indicates for the first half of July that the ice covered areas to the south (to the right) of Novaja Zemlja are connected to the polar ice cap through a narrow tongue of ice towards Frans Josefs Land. This feature is greatly supported by the ARTIST analysis and also other smaller details can be seen in both analyses. This tongue of ice has completely disappeared in the first half of August which can be seen in the CM-SAF analysis as well as in the ARTIST analysis. There is also a striking similarity of several details in the two analyses in August. Furthermore, the ice edge to the north of Svalbard is now well depicted also in the CM-SAF analysis as a contrast to in July when this part was too cloudy to reveal the ice extent.

We conclude that, despite of the simplicity of the used ice extent analysis method, it is possible to make a realistic analysis of the maximum ice extent by using cloud screening results from the CM-SAF method. This also implies that the prospect of making sea ice albedo estimations is feasible.

It is worth mentioning that the alternative method for ice detection based on the use of a more stringent cloudmask (previously presented in section 5.5) could unfortunately not be used here since it did not generate a large enough dataset with cloudfree pixels. However, the method could be suitable for future applications having access to a higher temporal resolution of satellite data (a large number of AVHRR overpasses per day).

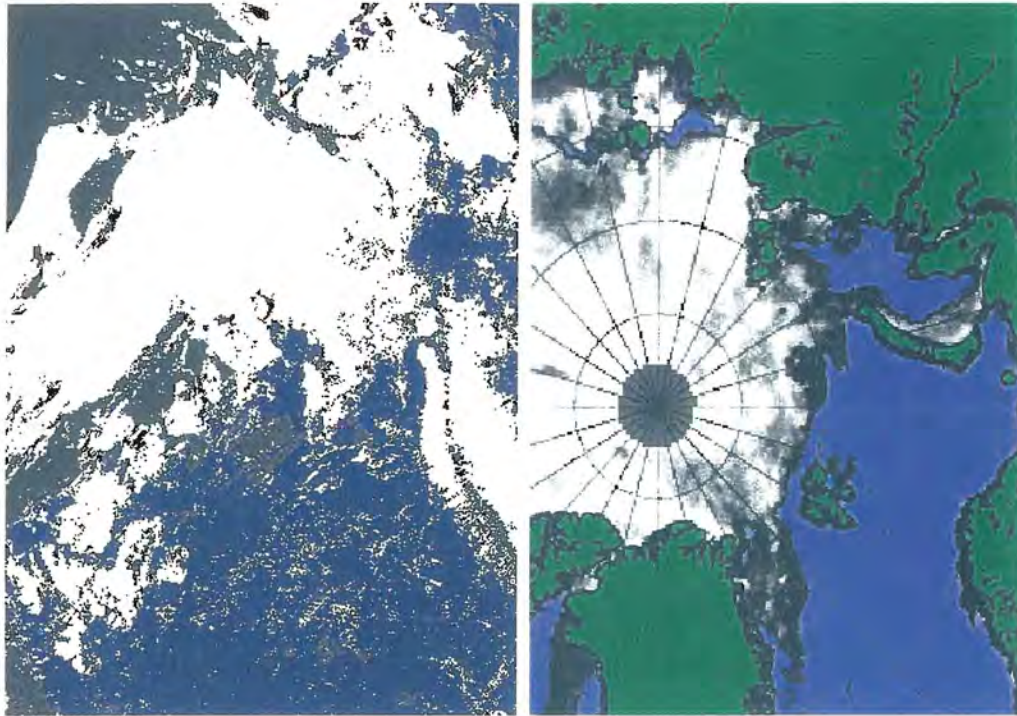


Figure 30: LEFT:Maximum ice extent (white pixels) in processing area ARC1KM.EAST analysed from AVHRR scenes in the period 2-15 July 2001. Blue pixels denote areas with open water and grey pixels areas where no cloud-free situations were found. RIGHT: SSM/I sea ice concentrations July 10 2001 from the ARTIST Sea Ice Algorithm at 12 km resolution. (Courtesy of Lars Kaleschke, Institute of Environmental Physics (iup) and Remote Sensing (ife), Dept. of Physics and Electrical Engineering, FB1 P.O. Box 330440, D-28334 Bremen,Germany - see also [www.seaice.de](http://www.seaice.de))

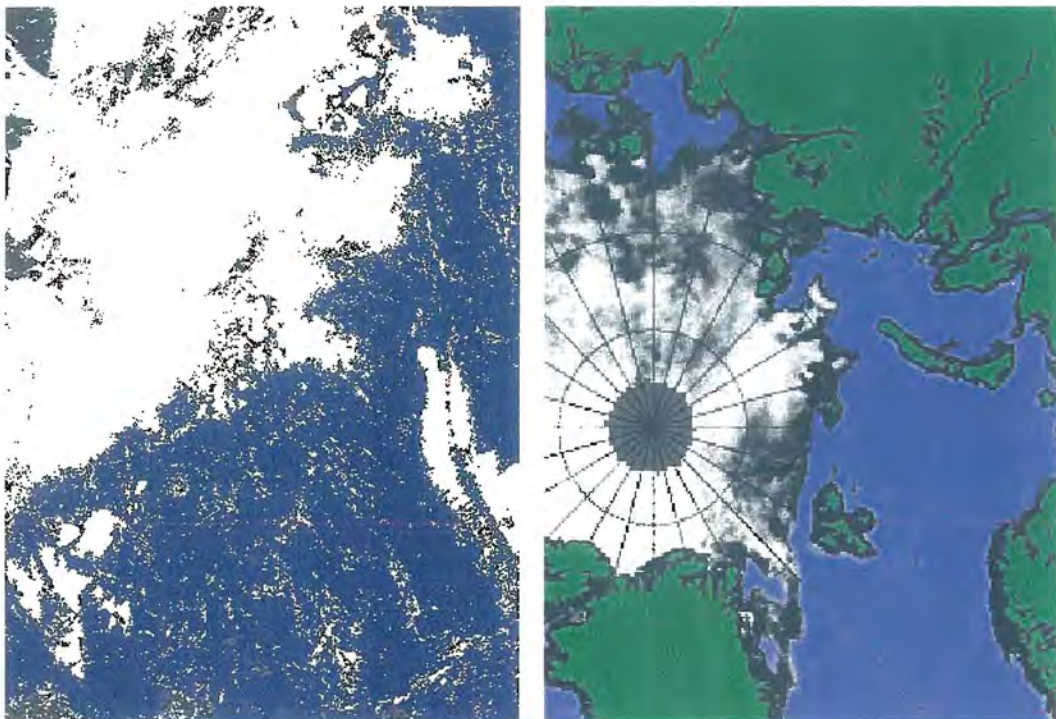


Figure 31: Same as in Fig. 30 but for the period 1-15 August and with the ARTIST SSM/I sea ice concentrations for August 10 2001.

## 13 Conclusions

The CM-SAF cloud detection algorithm results over two inner Arctic test areas based on NOAA-16 and NOAA-14 measurements during July and August 2001 have been studied by means of different intercomparisons. Results indicate some modifications which may be useful for getting a more accurate and flexible inner Arctic CM-SAF cloud scheme. Two of them are rather general.

- Cloud monitoring and use of cloud products for radiation budget calculations etc need a specified cloud definition. The traditional (descriptive) form (a set of water drops or ice crystals in the atmosphere) is insufficient. A quantitative basis of the definition should be implemented in order to guarantee a basis for both comparison of various detection methods and calculation of radiative effects of clouds. Satellite datasets are the only source to search for such a quantitative basis. The task is certainly not simple but unavoidable. In the class of threshold methods some progress to that direction can be achieved by means of precisely defined thresholds. But the precise definition itself may not be sufficient. Comparison of  $t_{45}$  values from different authors showed that the problem is still complicated. If the right threshold value is a function of local temperature, water vapor and viewing geometry one is unable to define it for wider use. *Vice versa*, the right threshold is valid for the (right) local conditions only. This leads to the conclusion that cloud products are comparable only if they are separated using right local thresholds. To solve the problem, any reliable method for measuring water vapor content simultaneously with AVHRR measurements is necessary.
- The cloud mask as a tool to separate perfectly clear and cloud contaminated pixels is important for calculating radiative properties for the underlying surface. Using cloud contaminated pixels for the latter operation leads to some bias in the final products. Similarly, an overcast mask should be introduced in order to assure non-biased radiative property calculations for clouds. Thus, a logical way of presenting results is in three groups: cloud, clear and mixture (or partially covered pixels). Pixels from the latter group should be kept away from calculations of cloud top temperature, optical thickness etc. There are several statistical approaches to estimate their contribution to the total cloud amount (Stowe 1999, Kärner 2000, Mattsson and Karlsson 2002). Keeping the type 19 (fractional or subpixel cloud) in the classification means that the authors are obliged to present also other parameters (e.g optical thickness) for that type. An alternative way is to consider types 19 (and may be also 15) as a mixture of clear and cloudy (optical) parameters. In that case one needs to focus on giving the most accurate algorithms how to use mixtures in applications, such as computing the radiation budget at the surface etc.
- Cloud mask results were tested using a few Oden and station observations during almost cloud-free situations over their vicinity. The results show good performance, in general, together with recalling that rare fog, (mist haze) is often classified as stratiform cloud (NOAA-16 over Oden in July 28). The results are easily understandable for a remote sensing specialist, but less acceptable by a ground meteorologist who often can see the sky through some rare haze. A more difficult problem for shortwave channels 3A and 3B is a considerably increased reflection sometimes during obviously cloud-free scenes. Spangenberg et al. (2001) have found that one possible reason is haze in case of CH3B. Histograms for  $R_{31}$ , collected in the present study show that strong increase in CH3A reflectance (leading to the values  $R_{31} > 1$ ) is often seen in clear cases over ice-free water and land. This may indicate that haze alone is not the single reason for misidentification. One possibility could be the existence of shadows on low clouds produced by higher clouds in situations with high solar zenith angles and which sometimes are mis-classified as cloudfree pixels. These shadows on clouds may distort 'normal' cloud reflection behaviour (as anticipated by the cloud detection method) and the corresponding relations between reflection in shortwave channels and near infrared channels.
- CH3A appears to be very useful tool (and thus, confirming the main goal for its application) for cloud mask determination over snow and ice. The statement is supported by Table 7 which shows that for the sub-area A all CM-SAF determined clear pixels have  $R_{31} < 0.3$  and low number (less than 3% of the observed amount) of pixels having that property is defined cloudy by CM-SAF. Comparison of CH3A and CH3B performance over that sub-area was impossible due to minimal common area.
- Direct comparison of CH3A and CH3B performances for cloud mask determination over mixed surfaces shows some advantage of CH3B, due to very low and still decreasing (empirical) prob-

ability estimate to find clear pixels if dT34 exceeds 24K. In case of  $R_{31}$  the corresponding probability decreases very slowly over all the range (compare Figures 12 and 13).

- The conditions  $R_{31} < 0.12$  and  $dT34 < 3$  K showed an ability to extract cloud-free pixels at a high level of confidence (in comparison of those determined by CM-SAF) for NOAA-16 and NOAA-14 datasets, respectively. The term high confidence means here very low per cent of misclassifications by these conditions. The ability can be further used for modifying the cloud detection method.
- The ability, mentioned in the previous item can be used for producing additional information to test for possible biases in NWP temperature and water vapor data caused by too low resolution grid or simple prediction errors. A more detailed proposal here can be found in the following section 13.1.
- CM-SAF is probably the first method enabling to produce large scale cloud type distribution in the arctic conditions. Such a dataset is extremely valuable for developing radiation budget calculation methods. At the first approximation the types look reasonable and can be used for further studies.
- The extracted cloud top heights for low-level cloud types showed that the cloud top method had serious deficiencies that must be improved. This problem was due to a coding error and a solution to the problem was described and demonstrated in section 11. However, future studies are necessary to make a thorough evaluation of the full impact of this upgrade of the method.
- A detailed study of the situations when very low and low opaque clouds (together with a part of medium level stratiform clouds) have very close T4-T<sub>s</sub> distribution is also necessary. The apparently too small difference between very thin and thick cirrus types present must also be further investigated.
- The main objective of this study was to investigate the feasibility of an Inner Arctic Cloud mask as produced by the current CM-SAF cloud algorithm. The validation efforts and inter-comparisons performed suggest a reasonable performance which does not deviate much from the performance previously experienced in other regions. However, some evidence of a slightly reduced performance in the Inner Arctic region has been noticed. A small fraction of all existing clouds appears to have remained undetected. The problem appears to be closely linked to the general occurrence of quite high solar zenith angles which frequently cause shadows on the surface of the earth but also, which is more serious, on surfaces of low-level clouds. This distorts the typical spectral appearance of clouds and may result in leaving them undetected. A future upgrade of the CM-SAF algorithm must especially take this problem into account.
- Realistic maximum ice extent analyses for limited periods during the studied two months have been demonstrated by use of CM-SAF cloudmask results and a simple interpretation of visible AVHRR radiances. This implies that the prospect of performing Inner Arctic sea ice albedo estimations should be feasible during the northern Hemisphere summer season provided that some precaution measures are taken to avoid contamination of result by spurious remaining cloud contamination.
- The entire processed Arctic dataset (including basic calibrated AVHRR channels, Cloud Mask and Cloud Type results) on area ARC1KM\_EAST could be made available in the HDF5 format on CD-ROMs for further studies.

### 13.1 Proposal for correction of NWP modelled surface temperatures in threshold preparation

The threshold for T4 has been very important in the whole history of satellite cloud detection. It is important also in the Arctic. In CM-SAF it is calculated using NWP surface temperature data which are submitted over a (comparatively) sparse grid in comparison with 1 km pixel size. This means that the NWP information is probably too smooth for proper use at the pixel level. Analysis of the AVHRR/3 data showed that the feature  $R_{31} < \alpha$  can be used to extract a certain set (hereafter CCL) of pixels, which, with high probability, contains only cloudfree ones. In the present study, mainly the value  $\alpha=0.12$  has been used, but some increase up to 0.15 may be reasonable also. The extracted set enables us to introduce an independent (on NWP data) scheme for indirect testing the fitness of the

precalculated  $T_s+t4$ ,  $t45$  and  $r06$  values for the current atmospheric state over the CCL. A provisional list of activities might be as follows:

- Calculate the difference  $x$  by formula (1) over the extracted pixels. If a sufficiently large bias is found, a new threshold for T4 should be calculated. There are several possible ways to do that. An important advantage is in the possibility of using land-mask to separate CCL set into land and sea pixels. Table 11 shows, that such a separation should lead to more flexible spatial resolution for the necessary thresholds. A preliminary statistical study of the range of actual deviations would be useful in order to determine the limit from what the bias will be large enough. Extrapolating the land and sea part of CCL set T4 values over the whole area, if necessary, gets an updated version for clear sky CH4 brightness temperature. Similar statistical reasoning to that of for precalculations can help to calculate new levels for the previous  $T_s+t4$  values.
- A direct comparison of precalculated  $t45$  and actual  $dT45$  over the CCL set should indicate whether their interrelation is logical (i.e  $dT45 < t45$ ) or not. If not, there are two ways to compensate – changing temperature or water vapor content. The possible decision depends on that for the previous item.
- Similar comparison can be produced for  $r06$  and R1 over the CCL set in order to test their accordance. This comparison can give important information for the method in the Arctic due to generally low solar elevation. Because of variations in the atmospheric humidity and aerosol content any theoretical dependence of R1 on SZA is questionable if SZA is higher than  $75^\circ$ .

A similar use based on feature  $dT34$  could be imagined for previous satellites with the old AVHRR/2 sensor. However, the greatest need of an update of used NWP-modelled surface temperatures is probably seen for night-time conditions (dark conditions) when the classification process is forced to make exclusive use of infrared data. It is at present difficult to assess whether the  $dT34$  feature can be used also for this purpose. This could be a topic for extended future studies focused specifically on conditions during the Arctic winter season.

## Acknowledgments

The authors thank Adam Dybbroe and Jenny Mattsson for computing assistance and useful discussions. OK thanks the SMHI administration for excellent living and working conditions during his stay.

## 14 References

- Ångström, 1924: Solar and terrestrial radiation. *Quart. J. Roy. Met. Soc.* **50**, 121-130.
- Appleman, H.S., 1962: A comparison of simultaneous aircraft and surface cloud observations. *J. Appl. Meteor.* **1**, 548-551.
- Avaste O., Ü. Mullamaa, H. Niilisk, M. Sulev, 1972: On coverage of the sky with clouds. In *Teploobmen v atmosfere*, Moscow, Nauka, 134-139. (in Russian).
- Chakrapani V., D.A. Spangenberg, et al. 2001: Improvements in AVHRR Daytime cloud detection over the ARM NSA site. Eleventh ARM Science Team Meeting Proceedings, Atlanta, Georgia, March 19-23, 2001.
- Dybbroe A., K.-G. Karlsson, M. Moberg and A. Thoss, 2000: Scientific Report for the SAFNWC Mid Term Review, SAF/NWC/SMHI/MTR/SR, SMHI, Issue 1.0, February 21, 2000, 148 pp.
- Dybbroe, A., M. Moberg, and A. Thoss, 2002: Proceedings of the Workshop for SAFNWC PPS software package beta Users, SMHI, April 11-12, 2002.
- Dybbroe A., A. Thoss, K-G. Karlsson, 2003: AVHRR cloud detection and analysis using dynamic thresholds and radiative transfer modelling. Submitted to *J. Appl. Meteor.*
- Dybbroe A., A. Thoss, K-G. Karlsson, 1999: The AVHRR cloud mask scheme of the SAF NWC. Proceedings of the Eumetsat satellite data users conference.

- Falls, L.W., 1974: The beta-distribution: a statistical model for world cloud cover. *J. Geophys. Res.* **79**, 1261-1264.
- Hyvärinen, O., K-G. Karlsson, A. Dybbroe, 1999: Investigations of NOAA AVHRR/3 1.6 $\mu$ m imagery for snow, cloud and sunglint discrimination. Nowcasting SAF Visiting scientist report, SMHI. 33 pp.
- Inoue T., 1987: A cloud type classification with NOAA 7 split-window measurements. *J. Geophys. Res.* **D92**, 3991-4000.
- Kaleschke, L., C. Lpkes, T. Vihma, J. Haarpaintner, A. Bochert, J. Hartmann, and G. Heygster, 2001: SSM/I Sea Ice Remote Sensing for Mesoscale Ocean-Atmosphere Interaction Analysis, *Canadian Journal of Remote Sensing* , **27**, No. 5, 526-537.
- Karlsson K-G., 1996: Cloud classifications with the SCANDIA model. SMHI Report Meteorology and Climatology, No 67, 36 pp.
- Karlsson K-G., 2001: A NOAA AVHRR cloud climatology over Scandinavia covering the period 1991-2000. SMHI Report Meteorology and Climatology, No 97, 95 pp.
- Karlsson K-G., 2003: A ten-year cloud climatology over Scandinavia derived from NOAA AVHRR imagery, to appear in *Int. J. of Climatology*.
- Kärner O., 2000: A multi-dimensional histogram technique for cloud classification. *Int. J. Remote Sensing*, **21**, 2463-2478.
- Kärner O., L. Di Girolamo, 2001: On automatic cloud detection over ocean *Int. J. Remote Sensing*, **22**, 3047-3052.
- Kärner O. and S. Keevallik, 1993: *Effective Cloud Cover Variations* A. Deepak Publishing, Hampton, VI, 210 pp.
- Key J.R., 2002: The cloud and surface parameter retrieval (CASPR) system for polar AVHRR User's Guide. Cooperative Institute for Meteorological Satellite Studies, University of Wisconsin-Madison, 61pp.
- Lund I.A., 1965: Estimating the probability of clear lines-of-sight from sunshine and cloud cover observations. *J. Appl. Meteor.* **4**, 714-722.
- Malberg, H. 1973: Comparison of mean cloud cover obtained by satellite photographs and ground-based observations over Europe and Atlantic. *Mon. Wea. Rev.* **101**, 893-897.
- Mattsson J., K-G. Karlsson, 2002: Cloud products feasibility study in the inner Arctic region. Part I: Cloud mask studies during the 2001 Oden Arctic expedition. Climate Monitoring SAF visiting scientist report, SMHI, 27pp.
- Matveyev L.T. (ed), 1986: *Global Cloud Field* Gidrometeoizdat, Leningrad, 280 pp. (in Russian)
- Minnis P., V. Chakrapani, D.R. Doelling et al. 2001: Cloud coverage and height during arctic FIRE ACE derived from AVHRR data. *J. Geophys. Res.* **106**, 15215-15232.
- Murata A. and T. Yamanouchi 1997: Distribution characteristics of clouds over East Antarctica in 1987 obtained from AVHRR. *J. Meteorol. Soc. Japan*, **75**, 81-93.
- Oancea, S., K. Andersson and K.-G. Karlsson, 2002: Validation of Arctic albedo measurements, CM-SAF Visiting Scientist Report, FMI, 20 pp.
- Rossow, W.B., and R.A. Schiffer, 1991: ISCCP cloud data products. *Bull. Amer. Meteor. Soc.*, **72**, 2-20.
- Saunders R.W., and K.T. Kriebel, 1988: An improved method for detecting clear sky and cloudy radiances from AVHRR data. *Int. J. Remote Sensing*, **9**, 123-150.
- Schweiger A.J., R.W.Lindsay, J.R.Key, J.A. Francis, 1999: Arctic clouds in multiyear satellite data sets. *Geoph. Res. Lett.* **26**, 1845-1848.

- Spangenberg D.A., V. Chakrapani, D.R. Doelling, P. Minnis, R.F. Arduini, 2001: Development of an automated arctic cloud mask using clear-sky satellite observations taken over the SHEBA and ARM NSA sites. Proc. 6th Conf. on Polar Meteorology and Oceanography, San Diego, CA, May 14-18, 2001, 246-249.
- Stephens, G.L. 1978: Radiation profiles of extended water clouds. *J. Atmos. Sci.*, **35**, 2123-2132.
- Stowe L.L., et al. 1988: Nimbus-7 global cloud climatology, Part 1: Algorithm and validation. *J. Climate* **1**, 445-470.
- Stowe L.L., et al. 1989: Nimbus-7 global cloud climatology, Part 2: First year results. *J. Climate* **2**, 672-709.
- Stowe L.L., P.A. Davis, and E.P. McClain, 1999: Scientific basis and initial evaluation of the CLAVR-1 global clear/cloud classification algorithm for the Advanced Very High Resolution Radiometer. *Journ. Atm. Ocean Techn.* **16**, 656-681.
- Trepte Q. R.F Arduini, et al., 2001: Development of a daytime polar cloud mask using theoretical models of near-infrared bidirectional reflectance for ARM and CERES. Proc. 6th Conf. on Polar Meteorology and Oceanography, San Diego, CA, May 14-18. 2001, 242-245.
- Yamanouchi, T., K.Suziki, and S. Kawaguchi, 1987: Detection of clouds in Antarctica from infrared multispectral data of AVHRR. *J. Meteorol. Soc. Japan*, **65**, 949-961.

## 15 Appendix

### 15.1 Used abbreviations

ACE - Arctic Cloud Experiment  
AVHRR - Advanced Very High Resolution Radiometer  
CH - channel  
ca - cloud amount (expressed in hundreths)  
cm - cloud mask (expressed in hundreths)  
CM-SAF - Climate Monitoring Satellite Application Facility  
FFS - Fifty-Fifty Split  
FIRE - First ISCCP Regional Experiment  
HIRLAM - High Resolution Limited Area Model  
ISCCP - International Satellite Cloud Climatology Project  
NASA - National Aeronautics and Space Agency  
NCI - Normalised Cloud Index  
NOAA - National Oceanic and Atmospheric Administration  
NWP - Numerical Weather Prediction  
RAZ - Relative AZimuth angle  
RTM - Radiative Transfer Model  
SAFNWC - Satellite Application Facility in support to Nowcasting and Very Short Range Forecasting  
SHEBA - Surface HEat Budget of the Arctic ocean  
SZA - Solar Zenith Angle  
TIGR - TOVS Initial Guess Retrieval database  
TOVS - Tiros Operational Vertical Sounder  
VZA - Viewing (scanning) Zenith Angle

Table 22: Comparison of station reports in nearly cloudless situations to NOAA-14 (top) and NOAA-16 (bottom) based CM-SAF products over 31×31 pixel areas

Date	GMT	LAT	LON	time diff min	octa	type	base height	cm by CM-SAF	types
3.07	12	77.0	15.5	18	1	Ci	150	0.27	15,19
		78.25	15.47	18	1	St	150	0.11	15,19
		72.37	52.7	18	0	-	-	0.01	15
12.07	12	77.0	15.5	26	1	-	1250	0.11	15,19
14.07	12	72.37	52.7	52	2	-	8000	0.01	19
16.07	12	78.92	11.93	27	2	-	150	0.21	15,19
20.07	12	80.62	58.05	21	2	Ci	8000	0.27	19
23.07	12	77.0	15.5	44	1	-	450	0.28	19
		78.92	11.93	44	1	-	800	0.2	19
		78.25	15.47	44	1	-	800	0.05	19
		80.62	58.05	44	0	-	-	0.99	9,19
		79.5	76.98	44	0	-	-	0	-
24.07	12	80.62	58.05	32	2	-	450	0.48	9,19
26.07	12	78.92	11.93	7	1	Ci	2250	0.18	15,19
31.07	09	78.25	15.47	49	1	Cs	800	0.15	15,19
3.08	09	76.5	25.07	90	2	-	800	0.02	19
5.08	12	78.25	15.47	12	1	-	1250	0.04	19
6.08	12	77.0	15.5	77	1	Cs	800	0.45	15,19
		78.25	15.47	77	2	Ci	8000	0.09	15,17
		72.37	52.7	37	2	-	3500	0.16	15,19
7.08	12	78.92	11.93	37	0	-	-	0.09	15,19
		78.25	15.47	37	0	-	-	0.07	15,19
		72.37	52.7	49	0	-	-	0	-
8.08	12	72.37	52.7	49	0	-	-	0	-
10.08	12	72.37	52.7	29	0	-	-	0.01	15,19
14.08	12	79.5	76.98	20	1	Ci	8000	0	-
20.08	12	80.62	58.05	9	1	Ci	8000	0.02	15,19
25.08	12	79.55	90.62	52	2	Ci	8000	0	-
26.08	12	77.0	15.5	65	1	-	3100	0.21	19
		79.55	90.62	65	2	Ci	3500	0.01	7
27.08	12	78.25	15.47	25	1	-	150	0.03	19
		72.37	52.7	25	1	-	800	0	-
28.08	12	77.0	15.5	13	2	Ci	150	0.22	7,19
		78.92	11.93	13	2	-	2250	0.06	19
		78.25	52.7	13	1	Ci	3500	0.02	15,19
23.07	9	77.0	15.5	23	1	-	800	0.22	19
6.08	9	77.0	15.5	23	2	Ci	8000	0.03	19
		78.25	15.47	23	1	Ci	800	0.09	19
7.08	9	78.25	15.47	34	0	-	-	0.07	19
		77.0	15.5	34	2	Ci	3500	0.09	19
21.08	9	76.5	25.07	21	2	-	150	0.13	19
26.08	9	77.0	15.5	32	2	-	450	0.30	7,19

Table 23: Cloud mask and cloud amount results for  $E$  sub-area by both satellites

Date	time diff min.	pixels	$cm_{16}$	$cm_{14}$	$ca_{16}$	$ca_{14}$	$ca_{216}$	$ca_{214}$
2.07	234	2204601	0.83	0.86	0.77	0.80	0.70	0.72
3.07	232	2190533	0.77	0.80	0.72	0.76	0.70	0.73
6.07	27	897311	0.37	0.46	0.33	0.42	0.29	0.35
10.07	9	1597731	0.92	0.92	0.86	0.87	0.83	0.80
11.07	8	1310766	0.94	0.93	0.85	0.86	0.80	0.74
11.07	94	926246	0.97	0.96	0.88	0.90	0.85	0.81
12.07	6	1373734	0.86	0.86	0.80	0.81	0.78	0.74
13.07	5	1449794	0.84	0.86	0.78	0.80	0.74	0.72
14.07	215	2056082	0.78	0.81	0.69	0.74	0.65	0.68
15.07	502	1516379	0.83	0.88	0.72	0.79	0.68	0.73
16.07	102	1651068	0.92	0.96	0.80	0.86	0.75	0.76
18.07	209	2246234	0.84	0.90	0.76	0.83	0.71	0.78
20.07	206	2272246	0.86	0.89	0.77	0.82	0.73	0.76
23.07	201	2079129	0.77	0.82	0.71	0.76	0.69	0.73
24.07	199	2174759	0.74	0.83	0.70	0.78	0.67	0.74
25.07	402	1485811	0.84	0.94	0.76	0.89	0.73	0.85
26.07	500	1209268	0.82	0.86	0.76	0.80	0.74	0.77
28.07	193	2359918	0.82	0.93	0.75	0.87	0.71	0.78
29.07	191	2365329	0.87	0.95	0.80	0.90	0.73	0.78
30.07	292	1878198	0.85	0.94	0.78	0.88	0.70	0.80
31.07	291	1952663	0.91	0.94	0.86	0.90	0.80	0.84
2.08	388	1664398	0.96	0.95	0.88	0.89	0.82	0.81
3.08	386	1556021	0.83	0.90	0.74	0.84	0.68	0.78
4.08	487	1373682	0.82	0.88	0.76	0.82	0.70	0.76
5.08	486	1344605	0.85	0.97	0.78	0.90	0.70	0.84
6.08	311	1958984	0.62	0.65	0.55	0.60	0.51	0.54
7.08	177	2345373	0.79	0.79	0.70	0.72	0.67	0.66
8.08	481	1129837	0.88	0.91	0.81	0.87	0.75	0.85
9.08	24	768786	0.57	0.68	0.54	0.65	0.53	0.63
10.08	275	2016791	0.58	0.68	0.52	0.62	0.49	0.59
13.08	168	2243785	0.84	0.88	0.77	0.82	0.70	0.74
14.08	167	2301579	0.78	0.82	0.73	0.78	0.65	0.68
15.08	33	934463	0.52	0.54	0.49	0.50	0.42	0.42
17.08	263	2085505	0.88	0.88	0.77	0.79	0.71	0.73
18.08	160	2280428	0.88	0.89	0.80	0.82	0.75	0.75
19.08	40	775320	0.88	0.87	0.81	0.80	0.78	0.75
20.08	259	2093085	0.72	0.79	0.69	0.77	0.66	0.74
21.08	155	1741008	0.79	0.83	0.74	0.78	0.68	0.70
23.08	46	1063383	0.68	0.69	0.59	0.61	0.54	0.53
24.08	352	2056082	0.79	0.78	0.70	0.73	0.62	0.66
25.08	149	2332993	0.56	0.58	0.51	0.53	0.48	0.50
26.08	147	2320407	0.58	0.58	0.54	0.55	0.52	0.52
27.08	248	2235903	0.73	0.75	0.68	0.71	0.65	0.68
28.08	247	2208955	0.77	0.78	0.72	0.75	0.70	0.73

## SMHIs publiceringar

SMHI ger ut sex rapportserier. Tre av dessa, R-serierna är avsedda för internationell publik och skrivs därför oftast på engelska. I de övriga serierna används det svenska språket.

Seriernas namn	Publiceras sedan
RMK (Rapport Meteorologi och Klimatologi)	1974
RH (Rapport Hydrologi)	1990
RO (Rapport Oceanografi)	1986
METEOROLOGI	1985
HYDROLOGI	1985
OCEANOGRAFI	1985

I serien METEOROLOGI har tidigare utgivits:

1985

- |    |   |    |   |
|----|---|----|---|
| 1  | Hagmarker, A. (1985)<br>Satellitmeteorologi.  | 11 | Laurin, S., Bringfelt, B. (1985)<br>Spridningsmodell för kväveoxider i gatumiljö.   |
| 2  | Fredriksson, U., Persson, Ch., Laurin, S. (1985)<br>Helsingborgsluft.   | 12 | Persson, Ch., Wern, L. (1985)<br>Spridnings- och depositionsberäkningar för avfallsförbränningsanläggning i Sofielund.        |
| 3  | Persson, Ch., Wern, L. (1985)<br>Spridnings- och depositionsberäkningar för avfallsförbränningsanläggningar i Sofielund och Högdalen. | 13 | Persson, Ch., Wern, L. (1985)<br>Spridnings- och depositionsberäkningar för avfallsförbränningsanläggning i Högdalen.         |
| 4  | Kindell, S. (1985)<br>Spridningsberäkningar för SUPRAs anläggningar i Köping.   | 14 | Vedin, H., Andersson, C. (1985)<br>Extrema köldperioder i Stockholm.  |
| 5  | Andersson, C., Kvik, T. (1985)<br>Vindmätningar på tre platser på Gotland. Utvärdering nr 1.  | 15 | Krieg, R., Omstedt, G. (1985)<br>Spridningsberäkningar för Volvos planerade bilfabrik i Uddevalla.                            |
| 6  | Kindell, S. (1985)<br>Spridningsberäkningar för Ericsson, Ingelstafabriken.   | 16 | Kindell, S. Wern, L. (1985)<br>Luftvårdsstudie avseende industrikombinatet i Nynäshamn (koncentrations- och luktberäkningar). |
| 7  | Fredriksson, U. (1985)<br>Spridningsberäkningar för olika plymlyft vid avfallsvärmeverket Sävenäs.                                    | 17 | Laurin, S., Persson, Ch. (1985)<br>Beräknad formaldehydspridning och deposition från SWEDSPANs spånskivefabrik.               |
| 8  | Fredriksson, U., Persson, Ch. (1985)<br>NO <sub>x</sub> - och NO <sub>2</sub> -beräkningar vid Vasaterminalen i Stockholm.            | 18 | Persson, Ch., Wern, L. (1985)<br>Luftvårdsstudie avseende industrikombinatet i Nynäshamn – depositionsberäkningar av koldamm. |
| 9  | Wern, L. (1985)<br>Spridningsberäkningar för ASEA transformers i Ludvika.   | 19 | Fredriksson, U. (1985)<br>Luktberäkningar för Bofors Plast i Ljungby, II.   |
| 10 | Axelsson, G., Eklind, R. (1985)<br>Ovädret på Östersjön 23 juli 1985.   |    |   |

- 20 Wern, L., Omstedt, G. (1985)  
Spridningsberäkningar för Volvos planerade bilfabrik i Uddevalla - energicentralen.
- 21 Krieg, R., Omstedt, G. (1985)  
Spridningsberäkningar för Volvos planerade bilfabrik i Uddevalla - kompletterande beräkningar för fabrikena.
- 22 Karlsson, K.-G. (1985)  
Information från Meteosat - forskningsrön och operationell tillämpning.
- 23 Fredriksson, U. (1985)  
Spridningsberäkningar för AB Åkerlund & Rausings fabrik i Lund.
- 24 Färnlöf, S. (1985)  
Radarmeteorologi.
- 25 Ahlström, B., Salomonsson, G. (1985)  
Resultat av 5-dygnsprognos till ledning för isbrytarverksamhet vintern 1984-85.
- 26 Wern, L. (1985)  
Avesta stadsmodell.
- 27 Hultberg, H. (1985)  
Statistisk prognos av ytemperatur.
- 1986
- 1 Krieg, R., Johansson, L., Andersson, C. (1986)  
Vindmätningar i höga master, kvartalsrapport 3/1985.
- 2 Olsson, L.-E., Kindell, S. (1986)  
Air pollution impact assessment for the SABAH timber, pulp and paper complex.
- 3 Ivarsson, K.-I. (1986)  
Resultat av byggväderprognoser - säsongen 1984/85.
- 4 Persson, Ch., Robertson, L. (1986)  
Spridnings- och depositionsberäkningar för en sopförbränningsanläggning i Skövde.
- 5 Laurin, S. (1986)  
Bilavgaser vid intagsplan - Eskilstuna.
- 6 Robertson, L. (1986)  
Koncentrations- och depositionsberäkningar för en sopförbränningsanläggning vid Ryaverken i Borås.
- 7 Laurin, S. (1986)  
Luften i Avesta - föroreningsbidrag från trafiken.
- 8 Robertson, L., Ring, S. (1986)  
Spridningsberäkningar för bromcyan.
- 9 Wern, L. (1986)  
Extrema byvindar i Orrefors.
- 10 Robertson, L. (1986)  
Koncentrations- och depositionsberäkningar för Halmstads avfallsförbränningsanläggning vid Kristinehed.
- 11 Törnevik, H., Ugnell (1986)  
Belastningsprognoser.
- 12 Joelsson, R. (1986)  
Något om användningen av numeriska prognoser på SMHI (i princip rapporten till ECMWF).
- 13 Krieg, R., Andersson, C. (1986)  
Vindmätningar i höga master, kvartalsrapport 4/1985.
- 14 Dahlgren, L. (1986)  
Solmätning vid SMHI.
- 15 Wern, L. (1986)  
Spridningsberäkningar för ett kraftvärmeverk i Sundbyberg.
- 16 Kindell, S. (1986)  
Spridningsberäkningar för Uddevallas fjärrvärmecentral i Hovhult.
- 17 Häggkvist, K., Persson, Ch., Robertson, L. (1986)  
Spridningsberäkningar rörande gasutsläpp från ett antal källor inom SSAB Luleåverken.
- 18 Krieg, R., Wern, L. (1986)  
En klimatstudie för Arlanda stad.
- 19 Vedin, H. (1986)  
Extrem arealnederbörd i Sverige.
- 20 Wern, L. (1986)  
Spridningsberäkningar för lösningsmedel i Tibro.
- 21 Krieg, R., Andersson, C. (1986)  
Vindmätningar i höga master - kvartalsrapport 1/1986.

- 22 Kvick, T. (1986)  
Beräkning av vindenergitillgången på några platser i Halland och Bohuslän.
- 23 Krieg, R., Andersson, C. (1986)  
Vindmätningar i höga master - kvartalsrapport 2/1986.
- 24 Persson, Ch. (SMHI), Rodhe, H. (MISU), De Geer, L.-E. (FOA) (1986)  
Tjernobylyockan - En meteorologisk analys av hur radioaktivitet spreds till Sverige.
- 25 Fredriksson, U. (1986)  
Spridningsberäkningar för Spendrups bryggeri, Grängesberg.
- 26 Krieg, R. (1986)  
Beräkningar av vindenergitillgången på några platser i Skåne.
- 27 Wern, L., Ring, S. (1986)  
Spridningsberäkningar, SSAB.
- 28 Wern, L., Ring, S. (1986)  
Spridningsberäkningar för ny ugn, SSAB II.
- 29 Wern, L. (1986)  
Spridningsberäkningar för Volvo Hallsbergverken.
- 30 Fredriksson, U. (1986)  
SO<sub>2</sub>-halter från Hammarbyverket kring ny arena vid Johanneshov.
- 31 Persson, Ch., Robertson, L., Häggkvist, K. (1986)  
Spridningsberäkningar, SSAB - Luleåverken.
- 32 Kindell, S., Ring, S. (1986)  
Spridningsberäkningar för SAABs planerade bilfabrik i Malmö.
- 33 Wern, L. (1986)  
Spridningsberäkningar för svavelsyrafabrik i Falun.
- 34 Wern, L., Ring, S. (1986)  
Spridningsberäkningar för Västhamnsverket HKV1 i Helsingborg.
- 35 Persson, Ch., Wern, L. (1986)  
Beräkningar av svaveldepositionen i Stockholmsområdet.
- 36 Joelsson, R. (1986)  
USAs månadsprognoser.
- 37 Vakant nr.
- 38 Krieg, R., Andersson, C. (1986)  
Utemiljön vid Kvarnberget, Lysekil.
- 39 Häggkvist, K. (1986)  
Spridningsberäkningar av freon 22 från Ropstens värmepumpverk.
- 40 Fredriksson, U. (1986)  
Vindklassificering av en plats på Hemsön.
- 41 Nilsson, S. (1986)  
Utvärdering av sommarens (1986) använda konvektionsprognoshjälpmedel.
- 42 Krieg, R., Kvick, T. (1986)  
Vindmätningar i höga master.
- 43 Krieg, R., Fredriksson, U. (1986)  
Vindarna över Sverige.
- 44 Robertson, L. (1986)  
Spridningsberäkningar rörande gasutsläpp vid ScanDust i Landskrona - bestämning av cyanvätehalter.
- 45 Kvick, T., Krieg, R., Robertson, L. (1986)  
Vindförhållandena i Sveriges kust- och havsband, rapport nr 2.
- 46 Fredriksson, U. (1986)  
Spridningsberäkningar för en planerad panncentral vid Lindsdal utanför Kalmar.
- 47 Fredriksson, U. (1986)  
Spridningsberäkningar för Volvo BMs fabrik i Landskrona.
- 48 Fredriksson, U. (1986)  
Spridningsberäkningar för ELMO-CALFs fabrik i Svenljunga.
- 49 Häggkvist, K. (1986)  
Spridningsberäkningar rörande gasutsläpp från syrgas- och bensenupplag inom SSAB Luleåverken.
- 50 Wern, L., Fredriksson, U., Ring, S. (1986)  
Spridningsberäkningar för lösningsmedel i Tidaholm.
- 51 Wern, L. (1986)  
Spridningsberäkningar för Volvo BM ABs anläggning i Braås.

- 52 Ericson, K. (1986)  
Meteorological measurements performed May 15, 1984, to June, 1984, by the SMHI.
- 53 Wern, L., Fredriksson, U. (1986)  
Spridningsberäkning för Kockums Plåtteknik, Ronneby.
- 54 Eriksson, B. (1986)  
Frekvensanalys av timvisa temperatur-observationer.
- 55 Wern, L., Kindell, S. (1986)  
Luktberäkningar för AB ELMO i Flen.
- 56 Robertson, L. (1986)  
Spridningsberäkningar rörande utsläpp av NO<sub>x</sub> inom Fagersta kommun.
- 57 Kindell, S. (1987)  
Luften i Nässjö.
- 58 Persson, Ch., Robertson, L. (1987)  
Spridningsberäkningar rörande gasutsläpp vid ScanDust i Landskrona - bestämning av cyanväte.
- 59 Bringfelt, B. (1987)  
Receptorbaserad partikelmodell för gatumiljömodell för en gata i Nyköping.
- 60 Robertson, L. (1987)  
Spridningsberäkningar för Varbergs kommun. Bestämning av halter av SO<sub>2</sub>, CO, NO<sub>x</sub> samt några kolväten.
- 61 Vedin, H., Andersson, C. (1987)  
E 66 - Linderödsåsen - klimatförhållanden.
- 62 Wern, L., Fredriksson, U. (1987)  
Spridningsberäkningar för Kockums Plåtteknik, Ronneby. 2.
- 63 Taesler, R., Andersson, C., Wallentin, C., Krieg, R. (1987)  
Klimatkorrigering för energiförbrukningen i ett eluppvärmt villaområde.
- 64 Fredriksson, U. (1987)  
Spridningsberäkningar för AB Åretå-Trycks planerade anläggning vid Kungens Kurva.
- 65 Melgarejo, J. (1987)  
Mesoskalig modellering vid SMHI.
- 66 Häggkvist, K. (1987)  
Vindlaster på kordahus vid Alviks Strand - numeriska beräkningar.
- 67 Persson, Ch. (1987)  
Beräkning av lukt och föroreningshalter i luft runt Neste Polyester i Nol.
- 68 Fredriksson, U., Krieg, R. (1987)  
En överskallig klimatstudie för Tornby, Linköping.
- 69 Häggkvist, K. (1987)  
En numerisk modell för beräkning av vertikal momentumtransport i områden med stora råhetsmoment. Tillämpning på ett energiskogsområde.
- 70 Lindström, Kjell (1987)  
Weather and flying briefing aspects.
- 71 Häggkvist, K. (1987)  
En numerisk modell för beräkning av vertikal momentumtransport i områden med stora råhetsmoment. En koefficientbestämning.
- 72 Liljas, E. (1988)  
Förbättrad väderinformation i jordbruket - behov och möjligheter (PROFARM).
- 73 Andersson, Tage (1988)  
Isbildning på flygplan.
- 74 Andersson, Tage (1988)  
Aeronautic wind shear and turbulence. A review for forecasts.
- 75 Kållberg, P. (1988)  
Parameterisering av diabatiska processer i numeriska prognosmodeller.
- 76 Vedin, H., Eriksson, B. (1988)  
Extrem arealnederbörd i Sverige 1881 - 1988.
- 77 Eriksson, B., Carlsson, B., Dahlström, B. (1989)  
Preliminär handledning för korrektion av nederbördsmängder.
- 78 Liljas, E. (1989)  
Torv-väder. Behovsanalys med avseende på väderprognoser och produktion av bränsletorv.
- 79 Hagmarker, A. (1991)  
Satellitmeteorologi.
- 80 Lövblad, G., Persson, Ch. (1991)  
Background report on air pollution situation in the Baltic states - a prefeasibility study.  
IVL Publikation B 1038.

- 81 Alexandersson, H., Karlström, C., Larsson-McCann, S. (1991)  
Temperaturen och nederbörden i Sverige 1961-90. Referensnormaler.
- 82 Vedin, H., Alexandersson, H., Persson, M. (1991)  
Utnyttjande av persistens i temperatur och nederbörd för vårflödesprognoser.
- 83 Moberg, A. (1992)  
Lufttemperaturen i Stockholm 1756 - 1990. Historik, inhomogeniteter och urbaniseringseffekt. Naturgeografiska Institutionen, Stockholms Universitet.
- 84 Josefsson, W. (1993)  
Normalvärden för perioden 1961-90 av globalstrålning och solskenstid i Sverige.
- 85 Laurin, S., Alexandersson, H. (1994)  
Några huvuddrag i det svenska temperatur-klimatet 1961 - 1990.
- 86 Fredriksson, U. och Ståhl, S. (1994)  
En jämförelse mellan automatiska och manuella fältmätningar av temperatur och nederbörd.
- 87 Alexandersson, H., Eggertsson Karlström, C. och Laurin S. (1997).  
Några huvuddrag i det svenska nederbördsklimatet 1961-1990.
- 88 Mattsson, J., Rummukainen, M. (1998)  
Växthuseffekten och klimatet i Norden - en översikt.
- 89 Kindbom, K., Sjöberg, K., Munthe, J., Peterson, K. (IVL) Persson, C. Roos, E., Bergström, R. (SMHI). (1998)  
Nationell miljöövervakning av luft- och nederbördskemi 1996.
- 90 Foltescu, V.L., Häggmark, L (1998)  
Jämförelse mellan observationer och fält med griddad klimatologisk information.
- 91 Hultgren, P., Dybbroe, A., Karlsson, K.-G. (1999)  
SCANDIA – its accuracy in classifying LOW CLOUDS
- 92 Hyvarinen, O., Karlsson, K.-G., Dybbroe, A. (1999)  
Investigations of NOAA AVHRR/3 1.6  $\mu\text{m}$  imagery for snow, cloud and sunglint discrimination (Nowcasting SAF)
- 93 Bennartz, R., Thoss, A., Dybbroe, A. and Michelson, D. B. (1999)  
Precipitation Analysis from AMSU (Nowcasting SAF)
- 94 Appelqvist, Peter och Anders Karlsson (1999)  
Nationell emissionsdatabas för utsläpp till luft - Förstudie.
- 95 Persson, Ch., Robertson L. (SMHI) Thaning, L (LFOA). (2000)  
Model for Simulation of Air and Ground Contamination Associated with Nuclear Weapons. An Emergency Preparedness Model.
- 96 Kindbom K., Svensson A., Sjöberg K., (IVL) Persson C., (SMHI) ( 2001)  
Nationell miljöövervakning av luft- och nederbördskemi 1997, 1998 och 1999.
- 97 Diamandi, A., Dybbroe, A. (2001)  
Nowcasting SAF  
Validation of AVHRR cloud products.
- 98 Foltescu V. L., Persson Ch. (2001)  
Beräkningar av moln- och dimdeposition i Sverigemodellen - Resultat för 1997 och 1998.
- 99 Alexandersson, H. och Eggertsson Karlström, C (2001)  
Temperaturen och nederbörden i Sverige 1961-1990. Referensnormaler - utgåva 2.
- 100 Korpela, A., Dybbroe, A., Thoss, A. (2001)  
Nowcasting SAF - Retrieving Cloud Top Temperature and Height in Semi-transparent and Fractional Cloudiness using AVHRR.
- 101 Josefsson, W. (1989)  
Computed global radiation using interpolated, gridded cloudiness from the MESA-BETA analysis compared to measured global radiation.
- 102 Foltescu, V., Gidhagen, L., Omstedt, G. (2001)  
Nomogram för uppskattning av halter av PM<sub>10</sub> och NO<sub>2</sub>
- 103 Omstedt, G., Gidhagen, L., Langner, J. (2002)  
Spridning av förbränningsemissioner från småskalig biobränsleeldning – analys av PM<sub>2.5</sub> data från Lycksele med hjälp av två Gaussiska spridningsmodeller.
- 104 Alexandersson, H. (2002)  
Temperatur och nederbörd i Sverige 1860 - 2001

- 105 Persson, Ch. (2002)  
Kvaliteten hos nederbördskemiska mätdata  
som utnyttjas för dataassimilation i  
MATCH-Sverige modellen".
- 106 Mattsson, J., Karlsson, K-G. (2002)  
CM-SAF cloud products feasibility study  
in the inner Arctic region  
Part I: Cloud mask studies during the 2001  
Oden Arctic expedition





Sveriges meteorologiska och hydrologiska institut  
601 76 Norrköping Tel 011-495 8000 Fax 011-495 8001  
[www.smhi.se](http://www.smhi.se)